Prandtl-Glauert-Lorentz based Absorbing Boundary Conditions for the convected Helmholtz equation

Hélène Barucq, Nathan Rouxelin, Sébastien Tordeux

Prandtl-Glauert-Lorentz based Absorbing Boundary Conditions for the convected Helmholtz equation

Hélène Barucq[a], Nathan Rouxelin[a,*], Sébastien Tordeux[a]

[a]*Makutu, Inria & E2S-UPPA, CNRS UMR 5142, France*

Abstract

We construct Absorbing Boundary Conditions (ABCs) for the convected Helmholtz equation. The construction is based upon the Prandtl-Glauert-Lorentz map which transforms the convected Helmholtz equation into the regular Helmholtz equations. The new ABCs are thus issued from classical Engquist-Majda ABCs and are valid for carrier flows that vary inside the domain but become uniform at infinity. They lead to accurate numerical results for low and intermediate Mach numbers and are easy to implement in an existing finite element or discontinuous Galerkin solver.

Keywords: convected Helmholtz equation, Absorbing Boundary Conditions, ABC, Prandtl Glauert Lorentz transformation

Introduction

Domain truncation is an important problem of computational wave dynamics. Indeed in many applications, the waves propagate in an infinite medium which must be truncated to a finite one to allow numerical simulation using finite element methods. The introduction of an artificial boundary should be treated carefully to avoid numerical pollution due to reflections at the boundary. Among others, the two most popular truncation techniques are

- *Perfectly Matched Layers (PMLs)*, introduced in [Ber94], which consist n surrounding the computational domain by a layer in which the waves are highly absorbed,
- *Absorbing Boundary Conditions (ABCs)*, introduced in [EM77], which consist which minimize the reflected waves generated by waves impinging the boundary introduced for truncating the computational domain.

It is worth remembering that ABCs are often expressed in terms of non-local operators and that finding local approximation of those operators is usually a challenging problem.

*Corresponding author

Email addresses: helene.barucq@inria.fr (Hélène Barucq), nathan.rouxelin@inria.fr (Nathan Rouxelin), sebastien.tordeux@inria.fr (Sébastien Tordeux)

In this paper we consider the *convected Helmholtz equation* which is the simplest model for acoustic wave propagation in a flow. It has been shown that standard PMLs are unstable because of the existence of back-propagating modes. In [BBL03], stable PMLs for the convected Helmholtz equation were derived, this work was generalized to more general configurations in [MBAG20]. The key ingredient of those stable PMLs is a change of variables that transforms the convected Helmholtz equation into the standard one. The so-called *Prandtl-Glauert-Lorentz transformation* (PGL) of [HPN19] is the most common example of such a change of variables. Similar work for time-domain acoustics has been performed in [DJ06]. On the other had, ABCs for the convected Helmholtz equation in a waveguide were derived in [Kim14] and [MAGB21]. For industrial applications in which an exact ABC is required, a FEM-BEM coupling that approximates the non-local Dirichlet-to-Neumann operator has been considered in [CES14, BCD+14].

Herein, we construct a family of local ABCs based on the *Prandtl-Glauert-Lorentz transformation* for the convected Helmholtz equation. Those ABCs are constructed from the ABCs formerly derived for the standard Helmholtz equation in [EM77]. As the *Prandtl-Glauert-Lorentz transformation* is only used to compute the impedance operator on the artificial boundary, the new ABCs are valid for a flow that varies inside the domain but becomes uniform at infinity. Those new ABCs are efficient for low and intermediate Mach numbers and are easy to implement in an existing finite-element solver.

This paper is organized as follows:

- in Section 1, we recall some results on the convected Helmholtz equation and precisely state the assumptions under which the new ABCs are derived,
- in Section 2, we use the *Prandtl-Glauert-Lorentz transformation* to construct the new ABCs,
- in Section 3, we present numerical results to illustrate the performance of the new ABCs.

1. Model problem and geometric settings

In this section, we introduce the *convected Helmholtz equation* and recall some of its properties. We also precisely state the assumptions under which the new Absorbing Boundary Condition are constructed. Finally, we show that on a bounded domain the convected Helmholtz equation with absorbing boundary conditions is a well-posed problem.

1.1. Equation and carrier flow

We consider the following *convected Helmholtz equation* written in pressure formulation

$$-\omega^2 p - 2i\omega \boldsymbol{v_0} \cdot \nabla p + \boldsymbol{v_0} \cdot \nabla[\boldsymbol{v_0} \cdot \nabla p] - \operatorname{div}\left(c_0^2 \nabla p\right) = s, \tag{1}$$

where p is the acoustic potential, $\boldsymbol{v_0}$ is the velocity of the carrier flow, c_0 is the adiabatic sound speed and s is the acoustic source.

In this paper, we use the following convention for time-harmonic solutions

$$\mathsf{p}(\boldsymbol{x}, t) = p(\boldsymbol{x}, \omega) e^{-i\omega t}. \tag{2}$$

To make the notations lighter, the $e^{-i\omega t}$ factor is omitted.

As there are several ways to write the convected Helmholtz equation, see [Pie90], we have chosen the simple form (1) as a model problem for this paper. The construction of the ABCs presented here can then be adapted to the other forms of the equation without major difficulties.

In this paper we will make the following usual assumptions on the carrier flow:

Assumption 1 (Conservation of mass). The velocity $\boldsymbol{v_0}$ satisfies the following mass conservation equation

$$\operatorname{div}(\boldsymbol{v_0}) = 0.$$

Assumption 2 (Subsonic flow). The carrier flow is subsonic, *ie.*

$$\inf_{\mathcal{O}} \left(c_0^2 - |\boldsymbol{v_0}|^2 \right) > 0.$$

We introduce the matrix

$$\boldsymbol{K_0} := c_0^2 \mathbf{Id} - \boldsymbol{v_0} \boldsymbol{v_0}^T,$$

using Assumption 1, (1) can be rewritten as

$$-\omega^2 p - \operatorname{div}\left(\boldsymbol{K_0} \nabla p + 2i\omega p \boldsymbol{v_0} \right) = s. \tag{3}$$

The quantity

$$\boldsymbol{\sigma} := -\boldsymbol{K_0} \nabla p - 2i\omega p \boldsymbol{v_0}$$

is called the *total flux* and will be convenient to derive absorbing boundary conditions. Indeed, let Γ be a curve and $\boldsymbol{n}_\Gamma$ its unitary normal vector, then the acoustic energy flux going through Γ is proportional to $\boldsymbol{\sigma}|_\Gamma \cdot \boldsymbol{n}_\Gamma$.

We have introduced the *total flux* $\boldsymbol{\sigma}$ which is a convenient quantity to work with mixed finite-element methods. However when working with continuous primal finite-element methods, it is possible to obtain a symmetric formulation, which would lead to an alternative boundary flux [HPN17, HPN19, LMG+20]. This flux is

$$\boldsymbol{g} := -c_0^2 \nabla p + (-i\omega p + \boldsymbol{v_0} \cdot \nabla p) \boldsymbol{v_0} = -\boldsymbol{K_0} \nabla p - i\omega p \boldsymbol{v_0}. \tag{4}$$

This alternative flux is related to $\boldsymbol{\sigma}$ by

$$\boldsymbol{g} = \boldsymbol{\sigma} + i\omega p \boldsymbol{v_0}. \tag{5}$$

1.2. Absorbing boundary condition, weak formulation and well-posedness

Equation (3) is posed on the free space $\mathbb{R}^n$ for $n = 2$ or 3. Even if we only present numerical examples in two dimensions, the ABCs derived in this paper are also valid in dimension 3. However to perform numerical simulation we need to work on a finite domain. In practice, we introduce a boundary Σ, the so-called artificial boundary, which limits a region including the support of the acoustic source and thus defines a bounded computational domain $\mathcal{O}$. The ABC is then set on the artificial boundary Σ.

There exists an exact boundary condition which makes the artificial boundary transparent. It can be written as

$$\boldsymbol{\sigma} \cdot \boldsymbol{n} + \mathrm{DtN}(p) = 0, \quad \text{on } \Sigma, \tag{6}$$

where DtN is the *Dirichlet-to-Neumann map* which is a non-local operator.

In this paper, we will approximate (6) by the following *local* absorbing boundary condition

$$\boldsymbol{\sigma} \cdot \boldsymbol{n} + \mathcal{Z} p = 0, \quad \text{on } \Sigma, \tag{7}$$

where $\mathcal{Z} \in \mathbb{C}$ is a local approximation of the DtN-operator which will be determined later.

The condition (7) has the form of an *impedance boundary condition* and we refer to $\mathcal{Z}$ as an *impedance-like coefficient*.

For now we will make the following assumption on $\mathcal{Z}$ and we will later show that it holds.

Assumption 3 (Value of $\mathcal{Z}$). The value of $\mathcal{Z}$ is chosen such that

$$\mathfrak{Im}\mathcal{Z} \neq \omega \boldsymbol{v_0} \cdot \boldsymbol{n}.$$

It is also possible to express the local ABC using the alternative flux $\boldsymbol{g}$ defined by (4)

$$\boldsymbol{g} \cdot \boldsymbol{n} + \mathcal{Z}_{\boldsymbol{g}} p = 0, \tag{8}$$

using (5) we immediately have

$$\mathcal{Z}_{\boldsymbol{g}} = \mathcal{Z} - i\omega \boldsymbol{v_0} \cdot \boldsymbol{n}. \tag{9}$$

Constructing an ABC expressed in terms of $\boldsymbol{\sigma}$ will therefore also lead to an ABC expressed in terms of $\boldsymbol{g}$.

Equation (3) and the impedance boundary condition (7) lead to the following problem:

$$\text{Seek } p \in H^1(\mathcal{O}) \text{ such that } \mathsf{a}(p, w) = \ell(w), \text{ for all } w \in H^1(\mathcal{O}), \tag{10}$$

where

$$\mathsf{a}(p, w) := \int_{\mathcal{O}} \boldsymbol{K_0} \nabla p \cdot \nabla w^* + 2i\omega p \boldsymbol{v_0} \cdot \nabla w^* - \omega^2 p w^* \mathrm{d}\boldsymbol{x} - \int_{\partial\mathcal{O}} \mathcal{Z} p w^* \mathrm{d}\sigma, \tag{11a}$$

$$\ell(w) := \int_{\mathcal{O}} s w^* \mathrm{d}\boldsymbol{x}. \tag{11b}$$

Notice that this formulation can only be obtained when Assumption 1 is true.

Before actually showing the well-posedness of the problem (10), we state the following lemma

Lemma 1. *Under* Assumption 1 *and if* $p \in H^1(\mathcal{O})$ *and* $\boldsymbol{b_0} \in \boldsymbol{L}^\infty(\mathcal{O}) \cap \boldsymbol{\mathcal{C}}(\mathcal{O})$*, the following identity holds*

$$\mathfrak{Re} \int_{\mathcal{O}} p \boldsymbol{v_0} \cdot \nabla p^* \mathrm{d}\boldsymbol{x} = \frac{1}{2} \int_{\partial\mathcal{O}} (\boldsymbol{v_0} \cdot \boldsymbol{n}) |p|^2 \mathrm{d}\sigma.$$

For the proof, we refer to [BRT21, Lemma 4.1].

Using this lemma, we can now prove that the convected Helmholtz equation with absorbing boundary conditions is a well-posed problem.

Theorem 2. *Under* Assumption 1, Assumption 2 *and* Assumption 3, *the problem* (10) *has a unique solution* $p \in H^1(\mathcal{O})$.

Proof. When Assumption 2 holds, $\boldsymbol{K_0}$ is a symmetric positive-definite matrix and its spectrum is given by

$$\mathrm{Sp}(\boldsymbol{K_0}) = \left\{ c_0^2, c_0^2 - |\boldsymbol{v_0}|^2 \right\}.$$

The problem (10) is therefore of Fredholm type and existence of the solution will follow from its uniqueness.

Taking $w = p$ in (11a) and $s = 0$ in (11b) leads to the following energy-like identity

$$\left\| \boldsymbol{K_0}^{\frac{1}{2}} \nabla p \right\|_{\mathcal{O}}^2 - \omega^2 \|p\|_{\mathcal{O}}^2 + 2i\omega \int_{\mathcal{O}} p \boldsymbol{v_0} \cdot \nabla p^* \mathrm{d}\boldsymbol{x} - \int_{\partial\mathcal{O}} \mathcal{Z} |p|^2 \mathrm{d}\sigma = 0, \tag{12}$$

where $\|\cdot\|_{\mathcal{O}}$ is the norm of $L^2(\mathcal{O})$.

Taking the imaginary part of (12) leads to

$$2\omega \mathfrak{Re} \int_{\mathcal{O}} p \boldsymbol{v_0} \cdot \nabla p^* \mathrm{d}\boldsymbol{x} - \mathfrak{Im} \int_{\partial\mathcal{O}} \mathcal{Z} |p|^2 \mathrm{d}\sigma = 0,$$

using Lemma 1, we have

$$\omega \int_{\partial\mathcal{O}} (\boldsymbol{v_0} \cdot \boldsymbol{n}) |p|^2 \mathrm{d}\sigma - \mathfrak{Im} \int_{\partial\mathcal{O}} \mathcal{Z} |p|^2 \mathrm{d}\sigma = 0,$$

which yields

$$\int_{\partial\mathcal{O}} (\omega \boldsymbol{v_0} \cdot \boldsymbol{n} - \mathfrak{Im}\mathcal{Z}) |p|^2 \mathrm{d}\sigma = 0,$$

and finally leads to $p|_{\partial\mathcal{O}} = 0$ if $\mathfrak{Im}\mathcal{Z} \neq \omega \boldsymbol{v_0} \cdot \boldsymbol{n}$.

On $\partial\mathcal{O}$ we have

$$\nabla p = (\partial_{\boldsymbol{n}} p) \boldsymbol{n} + \nabla_{\partial\mathcal{O}} p,$$

where $\nabla_{\partial\mathcal{O}}$ is the tangential gradient on $\partial\mathcal{O}$. As $p|_{\partial\mathcal{O}} = 0$, we have $\nabla_{\partial\mathcal{O}} p = 0$ and therefore

$$\nabla p = (\partial_{\boldsymbol{n}} p) \boldsymbol{n}.$$

Owing to boundary condition (7), we also have

$$\boldsymbol{\sigma} \cdot \boldsymbol{n} = 0,$$

and, as $p|_{\partial\mathcal{O}} = 0$,

$$0 = (\boldsymbol{K_0} \nabla p) \cdot \boldsymbol{n} = (\partial_{\boldsymbol{n}} p) \underbrace{\boldsymbol{n}^T \boldsymbol{K_0} \boldsymbol{n}}_{>0},$$

which finally leads to $\partial_{\boldsymbol{n}} p = 0$ as $\boldsymbol{K_0}$ is positive-definite.

Uniqueness of the solution now follows from the *unique continuation principle*, see [Pro59]. ∎

1.3. Geometric assumptions for the background flow

As the approximate radiation conditions will be constructed using the *Prandtl-Glauert-Lorentz transformation*, the background flow must be locally uniform around the artificial boundary. We therefore make the following assumption.

Assumption 4 (Uniform flow outside $\mathcal{O}$). There exists a compact $K \subsetneq \mathcal{O}$ such that $\boldsymbol{v_0}$ and c_0 are constant outside K.

A sketch of this configuration is given in FIGURE 1.

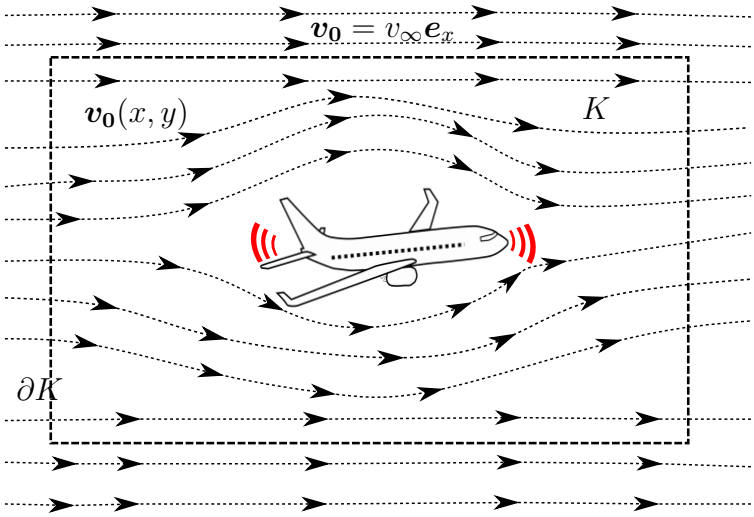

Figure 1: Flow around an aircraft, the flow is uniform outside of K

2. Prandtl-Glauert-Lorentz transformation and approximate ABCs

In this section we introduce the *Prandtl-Glauert-Lorentz transformation*, which is the main tool for the construction of the new ABCs. We recall that the *Prandtl-Glauert-Lorentz transformation* maps the convected Helmholtz equation into the standard one. As for the Helmholtz equation, the behaviour of the solution of the convected Helmholtz equation at infinity must be specified to ensure its uniqueness, leading to the notion of *outgoing solution*. In this section, we prove that the *Prandtl-Glauert-Lorentz transformation* of an outgoing solution is still an outgoing solution. We then show how the boundary conditions are transformed under this change of coordinates.

2.1. Prandtl-Glauert-Lorentz transformation

We define the *Lorentz factor*

$$\alpha := \sqrt{1 - M^2},$$

where M is the Mach-number defined as

$$\boldsymbol{M_0} := \frac{1}{c_0}\boldsymbol{v_0}, \quad \text{and} \quad M := |\boldsymbol{M_0}|.$$

Following [HPN19], we use the following transformation

$$\widetilde{t} = \alpha t + \frac{1}{\alpha c_0}(\boldsymbol{M_0} \cdot \boldsymbol{x}) \;\; ; \;\; \widetilde{\boldsymbol{x}} = \boldsymbol{A}\boldsymbol{x} := \left(\mathbf{Id} + \frac{1}{\alpha(1+\alpha)}\boldsymbol{M_0}\boldsymbol{M_0}^T\right)\boldsymbol{x}. \tag{13}$$

Depending on the sources, it can be called *Lorentz transformation*, *Prandtl-Glauert transformation* or sometimes *Prandtl-Glauert-Lorentz transformation*. The term *Lorentz transformation* is used as this transformation is close to the Lorentz transformation arising in special relativity.

Using the *Sherman-Morrisson formula* [SM50], it is easy to show that

$$\boldsymbol{A}^{-1} = \mathbf{Id} - \frac{1}{1+\alpha}\boldsymbol{M_0}\boldsymbol{M_0}^T.$$

We can therefore write the inverse *Prandtl-Glauert-Lorentz transformation*

$$t = \frac{1}{\alpha}\widetilde{t} - \frac{1}{\alpha c_0}(\boldsymbol{M_0} \cdot \widetilde{\boldsymbol{x}}) \;\; ; \;\; \boldsymbol{x} = \boldsymbol{A}^{-1}\widetilde{\boldsymbol{x}} := \left(\mathbf{Id} - \frac{1}{1+\alpha}\boldsymbol{M_0}\boldsymbol{M_0}^T\right)\widetilde{\boldsymbol{x}}. \tag{14}$$

2.2. Transformation of the convected Helmholtz equation

In this subsection, we prove that the *Prandtl-Glauert-Lorentz transformation* maps the convected Helmholtz equation to the standard Helmholtz equation. The material covered here is standard and can be found *eg.* in [HPN19]. We have added it here for the sake of completeness. We would like to point out that as the *Prandtl-Glauert-Lorentz transformation* is a spacetime transformation, it is easier to work in time-domain. Then we go back to the frequency domain thanks to a Fourier transform.

Let us consider the time-domain convected wave equation

$$(\partial_t + \boldsymbol{v_0} \cdot \nabla)^2 p - c_0^2 \Delta p = s. \tag{15}$$

Lemma 3. *If c_0 and $\boldsymbol{v_0}$ are constant, the quantity*

$$\widetilde{p}(\widetilde{\boldsymbol{x}}, \widetilde{t}) := p(\boldsymbol{x}, t), \tag{16}$$

satisfies the following wave equation

$$\partial^2_{\widetilde{t}\widetilde{t}}\widetilde{p} - c_0^2 \widetilde{\Delta}\widetilde{p} = \widetilde{s}, \tag{17}$$

where $\widetilde{\Delta}$ is the Laplace operator with respect to $\widetilde{\boldsymbol{x}}$ and $(\widetilde{\boldsymbol{x}}, \widetilde{t})$ is defined by (13).

PROOF. To make the proof more concise, we only consider the case where $\boldsymbol{M_0} = M\boldsymbol{e}_x$. The other cases reduce to this one by rotation. In this case, (15) can be rewritten as

$$\partial_{tt}^2 p + 2c_0 M \partial_{tx}^2 p - c_0^2 \left(1 - M^2\right) \partial_{xx}^2 p - c_0^2 \partial_{yy}^2 p = s, \tag{18}$$

and the Lorentz factor is still given by

$$\alpha = \sqrt{1 - M^2}.$$

Using the chain rule and (14), we have

$$\partial_{tt}^2 \widetilde{p} = \frac{1}{\alpha^2} \partial_{tt}^2 p, \tag{19a}$$

$$\partial_{\widetilde{x}\widetilde{x}}^2 \widetilde{p} = \frac{M^2}{\alpha^2 c_0^2} \partial_{tt}^2 p - \frac{2M}{\alpha c_0} \left(1 - \frac{M^2}{1+\alpha}\right) \partial_{tx}^2 p + \left(1 - \frac{M^2}{1+\alpha}\right)^2 \partial_{xx}^2 p, \tag{19b}$$

$$\partial_{\widetilde{y}\widetilde{y}}^2 \widetilde{p} = \partial_{yy}^2 p. \tag{19c}$$

We notice that

$$1 - \frac{M^2}{1+\alpha} = \frac{1 - M^2 + \alpha}{1+\alpha} = \frac{\alpha(1+\alpha)}{1+\alpha} = \alpha. \tag{20}$$

As (17) can be rewritten as

$$\partial_{tt}^2 \widetilde{p} - c_0^2 \partial_{\widetilde{x}\widetilde{x}}^2 \widetilde{p} - c_0^2 \partial_{\widetilde{y}\widetilde{y}}^2 \widetilde{p} = \widetilde{s},$$

using (19a)–(19b)–(19c) and (20) immediately leads to (18). ∎

We will now derive a relationship between the solutions in the frequency domain.

Lemma 4. *Let p be a solution of (3) and let $\widetilde{p}$ be defined by (16). If c_0 and $\boldsymbol{v_0}$ are constant, the following identity holds*

$$\mathcal{F}[\widetilde{p}](\widetilde{\boldsymbol{x}}, \widetilde{\omega}) = \alpha \exp\left[i\omega \frac{\boldsymbol{M_0} \cdot \boldsymbol{x}}{\alpha^2 c_0}\right] \mathcal{F}[p](\boldsymbol{x}, \omega), \tag{21}$$

where $\mathcal{F}$ denotes the Fourier transform with respect to time and the relationship between the frequencies is

$$\widetilde{\omega} = \frac{\omega}{\alpha}. \tag{22}$$

The same identity holds for the source-term s, ie.

$$\mathcal{F}[\widetilde{s}](\widetilde{\boldsymbol{x}}, \widetilde{\omega}) = \alpha \exp\left[i\omega \frac{\boldsymbol{M_0} \cdot \boldsymbol{x}}{\alpha^2 c_0}\right] \mathcal{F}[s](\boldsymbol{x}, \omega).$$

PROOF. As discussed in (2) we chose the $e^{-i\omega t}$ convention for time-harmonic solutions, we shall therefore use the following convention for the Fourier transform with respect to time

$$\mathcal{F}[p](\boldsymbol{x},\omega) := \int_{\mathbb{R}} p(\boldsymbol{x},t)e^{i\omega t}\mathrm{d}t.$$

Let us begin with the solution in Lorentz coordinates, the frequency domain solution is given by

$$\mathcal{F}[\widetilde{p}](\widetilde{\boldsymbol{x}},\widetilde{\omega}) = \int_{\mathbb{R}} \widetilde{p}(\widetilde{\boldsymbol{x}},\widetilde{t})e^{i\widetilde{\omega}\widetilde{t}}\mathrm{d}\widetilde{t},$$

and (13) implies

$$= \int_{\mathbb{R}} \widetilde{p}(\widetilde{\boldsymbol{x}},\widetilde{t})e^{i\widetilde{\omega}\alpha t}\exp\left(i\widetilde{\omega}\frac{\boldsymbol{M_0}\cdot\boldsymbol{x}}{\alpha c_0}\right)\alpha\mathrm{d}t,$$

and we have

$$= \alpha\exp\left(i\widetilde{\omega}\frac{\boldsymbol{M_0}\cdot\boldsymbol{x}}{\alpha c_0}\right)\int_{\mathbb{R}} p(\boldsymbol{x},t)e^{i\alpha\widetilde{\omega}t}\mathrm{d}t.$$

Finally, we get that

$$\mathcal{F}[\widetilde{p}](\widetilde{\boldsymbol{x}},\widetilde{\omega}) = \alpha\exp\left(i\widetilde{\omega}\frac{\boldsymbol{M_0}\cdot\boldsymbol{x}}{\alpha c_0}\right)\mathcal{F}[p](\boldsymbol{x},\alpha\widetilde{\omega}), \tag{23}$$

Taking $\omega = \alpha\widetilde{\omega}$ in (23) leads to (21) and (22). ∎

To summarize, when c_0 and $\boldsymbol{v_0}$ are constant, then LEMMA 3 and LEMMA 4 imply that the *Prandtl-Glauert-Lorentz transformation* maps the convected Helmholtz equation (3) into the following Helmholtz equation

$$-\left(\frac{\omega}{\alpha}\right)^2\widetilde{p} - c_0^2\widetilde{\Delta}\widetilde{p} = \widetilde{s}.$$

2.3. Transformation of the boundary condition

We will now show how the boundary conditions are changed under the *Prandtl-Glauert-Lorentz transformation*.

We denote by Σ the artificial boundary in physical coordinates and $\widetilde{\Sigma}$ the artificial boundary in Lorentz coordinates. We will chose a circle centered on the origin for $\widetilde{\Sigma}$, Σ will therefore be an ellipse. An example is depicted on FIGURE 2.

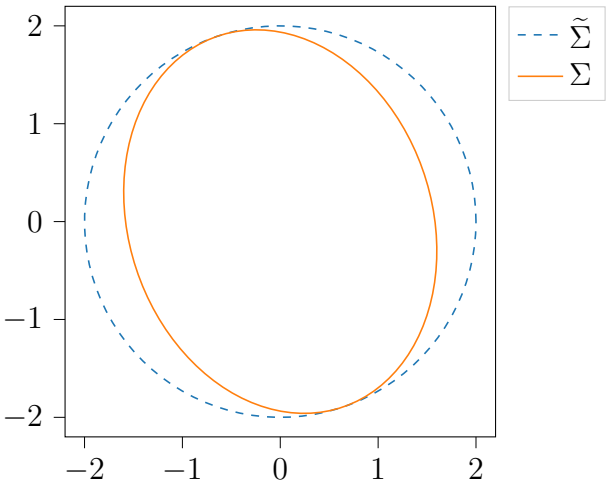

Figure 2: Σ and $\widetilde{\Sigma}$ for $\boldsymbol{M_0} = [0.6\ 0.2]^T$ and $R = 2$

More precisely, the following lemma holds.

Lemma 5. *Let $R > 0$. If the artificial boundary in Lorentz coordinates satisfies*

$$\widetilde{\Sigma} = \left\{ \widetilde{\boldsymbol{x}} \;\middle|\; |\widetilde{\boldsymbol{x}}|^2 = R^2 \right\} = \left\{ \widetilde{\boldsymbol{x}} = R\left(\cos(t)\boldsymbol{e}_x + \sin(t)\boldsymbol{e}_y\right) \;\middle|\; t \in \mathbb{S}^1 \right\},$$

then the artificial boundary in physical coordinates satisfies

$$\Sigma = \left\{ \boldsymbol{x} \;\middle|\; |\boldsymbol{A}\boldsymbol{x}| = R^2 \right\} = \left\{ \boldsymbol{x} = R\left(\cos(t)\boldsymbol{A}_1 + \sin(t)\boldsymbol{A}_2\right) \;\middle|\; t \in \mathbb{S}^1 \right\},$$

where $\boldsymbol{A}_1$ and $\boldsymbol{A}_2$ are the first and second columns of $\boldsymbol{A}^{-1}$.

Remark 2.1. At first glance, the other choice (taking a circle in physical coordinates and an ellipse in Lorentz coordinates) may seem more natural. However ABCs for the Helmholtz equation on an ellipsoid are more complicated to implement. If they are derived using an analytical point of view, those ABCs are expressed using special functions whose numerical evaluation may be unstable, see [BST12, Sai08]. On the other hand, if a geometric point of view is used, the resulting ABCs involve curvature operators that are difficult to approximate, see [BT80, ABB99].

We will now state and prove the main result of this paper.

Theorem 6. *Let p be the solution of*

$$-\omega^2 p - \operatorname{div}\left(\boldsymbol{K_0}\nabla p + 2i\omega\boldsymbol{v_0}\right) = s, \qquad \text{in } \mathcal{O}, \tag{24a}$$

$$\boldsymbol{\sigma}\cdot\boldsymbol{n} + \mathcal{Z}p = 0, \qquad \text{on } \Sigma, \tag{24b}$$

then if $\boldsymbol{v_0}$ and c_0 are constant, $\widetilde{p}$ defined by (21) satisfies

$$-\widetilde{\omega}^2\widetilde{p} - c_0^2\widetilde{\Delta}\widetilde{p} = \widetilde{s}, \qquad \text{in } \widetilde{\mathcal{O}}, \tag{25a}$$

$$\partial_{\widetilde{\boldsymbol{n}}}\widetilde{p} + \widetilde{\mathcal{Z}}\widetilde{p} = 0, \qquad \text{on } \widetilde{\Sigma}, \tag{25b}$$

if the impedance operators satisfy

$$\mathcal{Z}(\boldsymbol{x},\omega) = -\frac{c_0^2}{\mu}\widetilde{\mathcal{Z}}(\widetilde{\boldsymbol{x}},\widetilde{\omega}) + i\omega\boldsymbol{v_0}\cdot\boldsymbol{n}, \tag{26}$$

and $\mu := |\boldsymbol{A}^{-T}\boldsymbol{n}|^{-1}$ *is a scaling factor.*

Notice that even if THEOREM 6 is stated for a uniform flow, the new Absorbing Boundary Conditions can be used in the more general case described by ASSUMPTION 4. Indeed as the *Prandtl-Glauert-Lorentz transformation* will only be used to construct the impedance operator, the carrier flow only needs to be locally uniform close to the artificial boundary.

Remark 2.2. In (26) we can see that the impedance-like coefficient for the convected Helmholtz equation is the impedance coefficient of the standard Helmholtz equation scaled and shifted with a correction term that takes convection into account.

PROOF. The equivalence of the volumetric parts (24a) and (25a) is a direct consequence of LEMMA 3 and LEMMA 4. Let us now focus on the boundary conditions (24b) and (25b). This is adapted from [HPN19, Sec. 3].

We assume that Σ and $\widetilde{\Sigma}$ have the following cartesian equations

$$\Sigma : \{\Phi(\boldsymbol{x}) = 0\},$$
$$\widetilde{\Sigma} : \left\{\widetilde{\Phi}(\widetilde{\boldsymbol{x}}) = 0\right\}.$$

Step 1:

Because of the chain rule, we have the following relationship between their normal directions

$$\nabla\Phi = \frac{\partial\Phi}{\partial\boldsymbol{x}} = \frac{\partial\widetilde{\boldsymbol{x}}}{\partial\boldsymbol{x}}\frac{\partial\widetilde{\Phi}}{\partial\widetilde{\boldsymbol{x}}} = \boldsymbol{A}^T\widetilde{\nabla}\widetilde{\Phi} \tag{27}$$

Let $\boldsymbol{n}$ and $\widetilde{\boldsymbol{n}}$ be the unit normal vectors to Σ and $\widetilde{\Sigma}$ respectively. We have

$$\widetilde{\boldsymbol{n}} = \frac{1}{|\widetilde{\nabla}\widetilde{\Phi}|}\widetilde{\nabla}\widetilde{\Phi},$$

which becomes thanks to (27)

$$= \frac{1}{|\boldsymbol{A}^{-T}\nabla\Phi|}\boldsymbol{A}^{-T}\nabla\Phi,$$

then, since $\nabla\Phi = |\nabla\Phi|\boldsymbol{n}$, we have

$$= \frac{|\nabla\Phi|}{|\boldsymbol{A}^{-T}\nabla\Phi|}\boldsymbol{A}^{-T}\boldsymbol{n},$$

which implies

$$\widetilde{\boldsymbol{n}} = \mu\boldsymbol{A}^{-T}\boldsymbol{n},$$

where μ is a scaling factor that ensures that $|\widetilde{\boldsymbol{n}}| = 1$.

Step 2:

We have

$$\boldsymbol{A}^{-1}\boldsymbol{M_0} = \left(\mathbf{Id} - \frac{1}{1+\alpha}\boldsymbol{M_0}\boldsymbol{M_0}^T\right)\boldsymbol{M_0} = \left(1 - \frac{|\boldsymbol{M_0}|^2}{1+\alpha}\right)\boldsymbol{M_0} = \alpha\boldsymbol{M_0}.$$

Starting from [HPN19, Eq. (11)], multiplying by $\boldsymbol{A}^{-1}$ on the left and by $\boldsymbol{A}^{-T}$ on the right, we have

$$c_0^2\boldsymbol{M_0}\boldsymbol{M_0}^T - c_0^2\mathbf{Id} = -c_0^2\boldsymbol{A}^{-1}\boldsymbol{A}^{-T} \Longleftrightarrow \boldsymbol{A}^{-1}\boldsymbol{A}^{-T} = \mathbf{Id} - \boldsymbol{M_0}\boldsymbol{M_0}^T.$$

Step 3:

We recall that

$$\widetilde{p}(\widetilde{\boldsymbol{x}}, \widetilde{\omega}) = \alpha\alpha \exp\left[\frac{i\omega}{\alpha^2 c_0}\boldsymbol{M_0}\cdot\boldsymbol{x}\right] p(\boldsymbol{x}, \omega).$$

Using the chain rule, we have

$$\widetilde{\nabla}p = \boldsymbol{A}^{-T}\nabla p, \quad \text{and} \quad \widetilde{\nabla}\left[\alpha \exp\left[\frac{i\omega}{\alpha^2 c_0}\boldsymbol{M_0}\cdot\boldsymbol{x}\right]\right] = \frac{i\omega}{\alpha^2 c_0}\alpha \exp\left[\frac{i\omega}{\alpha^2 c_0}\boldsymbol{M_0}\cdot\boldsymbol{x}\right]\boldsymbol{A}^{-T}\boldsymbol{M_0},$$

and therefore

$$\begin{aligned}
\partial_{\widetilde{\boldsymbol{n}}}\widetilde{p} &= \widetilde{\boldsymbol{n}}\cdot\widetilde{\nabla}\widetilde{p} \\
&= \alpha \exp\left[\frac{i\omega}{\alpha^2 c_0}\boldsymbol{M_0}\cdot\boldsymbol{x}\right]\widetilde{\boldsymbol{n}}^T\left(\boldsymbol{A}^{-T}\nabla p + \frac{i\omega}{\alpha^2 c_0}p\boldsymbol{A}^{-T}\boldsymbol{M_0}\right) \\
&= \alpha \exp\left[\frac{i\omega}{\alpha^2 c_0}\boldsymbol{M_0}\cdot\boldsymbol{x}\right]\mu\boldsymbol{n}^T\boldsymbol{A}^{-1}\left(\boldsymbol{A}^{-T}\nabla p + \frac{i\omega}{\alpha c_0}p\boldsymbol{M_0}\right) \\
&= \alpha \exp\left[\frac{i\omega}{\alpha^2 c_0}\boldsymbol{M_0}\cdot\boldsymbol{x}\right]\mu\boldsymbol{n}^T\left((\mathbf{Id} - \boldsymbol{M_0}\boldsymbol{M_0}^T)\nabla p + i\frac{\omega}{c_0}p\boldsymbol{M_0}\right) \\
&= \alpha \exp\left[\frac{i\omega}{\alpha^2 c_0}\boldsymbol{M_0}\cdot\boldsymbol{x}\right]\frac{\mu}{c_0^2}\boldsymbol{n}^T\left(\underbrace{\boldsymbol{K_0}\nabla p + 2i\omega p\boldsymbol{v_0}}_{=-\boldsymbol{\sigma}} - i\omega p\boldsymbol{v_0}\right) \\
&= \alpha \exp\left[\frac{i\omega}{\alpha^2 c_0}\boldsymbol{M_0}\cdot\boldsymbol{x}\right]\frac{\mu}{c_0^2}\left(\mathcal{Z}p - i\omega p\boldsymbol{v_0}\cdot\boldsymbol{n}\right)
\end{aligned}$$

Using (26) and

$$p(\boldsymbol{x}, \omega) = \frac{1}{\alpha}\exp\left[\frac{-i\omega}{\alpha^2 c_0}\boldsymbol{M_0}\cdot\boldsymbol{x}\right]\widetilde{p}(\widetilde{\boldsymbol{x}}, \widetilde{\omega}),$$

we have

$$\partial_{\widetilde{\boldsymbol{n}}}\widetilde{p} = -\widetilde{\mathcal{Z}}\widetilde{p},$$

which concludes the proof. ∎

Remark 2.3. The minus sign in (26) comes from the fact that we have chosen to work with $\boldsymbol{\sigma} \cdot \boldsymbol{n}$ which should be interpreted as $-\partial_{\boldsymbol{n}} p$. It turns out that this choice of unknown is convenient for constructing mixed finite element methods, see [BRT21].

We recall that the alternative flux $\boldsymbol{g} = \boldsymbol{K_0} \nabla p + i\omega p \boldsymbol{v_0}$, defined in (4), is often use with primal finite-element methods. For this flux, the impedance boundary condition (8) reads

$$\boldsymbol{g} \cdot \boldsymbol{n} + \mathcal{Z}_{\boldsymbol{g}} p = 0,$$

and we recall that the identity (9), that is

$$\mathcal{Z}_{\boldsymbol{g}} = \mathcal{Z} - i\omega \boldsymbol{v_0} \cdot \boldsymbol{n}.$$

Corollary 1. *The impedance operator $\mathcal{Z}_{\boldsymbol{g}}$ satisfies*

$$\mathcal{Z}_{\boldsymbol{g}}(\boldsymbol{x}, \omega) = -\frac{c_0^2}{\mu} \widetilde{\mathcal{Z}}(\widetilde{\boldsymbol{x}}, \widetilde{\omega}).$$

2.4. Outgoing solutions of the convected Helmholtz equation

The existence of outgoing solutions for an equation is the key condition for obtaining absorbing conditions that can give well-posed boundary problems. In this section, we will prove that the notion of *outgoing solution* for the convected Helmholtz equation can be inherited from the one for the standard Helmholtz equation through the *Prandtl-Glauert-Lorentz transformation.*

Lemma 7. *The* Prandtl-Glauert-Lorentz transformation *maps outgoing solutions of the convected Helmholtz equation to outgoing solutions of the Helmholtz equation. More precisely, the following diagram is commutative*

$$\begin{array}{ccc} p_{conv}(\boldsymbol{x}, t) & \xrightarrow{t\to\infty} & p_{conv,\omega}(\boldsymbol{x}) \\ \Big\downarrow PGL_t & & PGL_\omega^{-1} \Big\uparrow \\ \widetilde{p}_{std}(\widetilde{\boldsymbol{x}}, \widetilde{t}) & \xrightarrow{\widetilde{t}\to\infty} & \widetilde{p}_{std,\widetilde{\omega}}(\widetilde{\boldsymbol{x}}) \end{array}$$

where p_{conv} and $\widetilde{p}_{std}$ are the time-domain solutions of the convected and standard wave equations, and $p_{conv,\omega}$ and $\widetilde{p}_{std,\widetilde{\omega}}$ are outgoing solutions of the convected and standard Helmholtz equations.

This result is proven by using the *limiting amplitude principle* which consists in studying the long-term behaviour of the time-domain solution with the following source term

$$g(\boldsymbol{x}, t) = \begin{cases} s(\boldsymbol{x}) e^{-i\omega t}, & \text{if } t > 0 \\ 0, & \text{if } t \leqslant 0 \end{cases},$$

where s is a function in $L^2(\mathcal{O})$ with compact support. As the proof of this lemma is rather long and technical, it is given in Appendix A.

2.5. New ABCs for the convected Helmholtz equation in 2D

In this section, we derive the practical values used for the impedance-like operators for the convected Helmholtz equation from Absorbing Boundary Conditions formerly derived for the Helmholtz equation.

2.5.1. Lorentz ABCs

In this section, we recall some absorbing boundary conditions on a circle for the Helmholtz equation. The ABCs of this section are specific to the 2D setting, however the extension to 3D is straightforward as the result of THEOREM 6 holds for any dimension. Those conditions will define the $\widetilde{\mathcal{Z}}$ operator applied on $\widetilde{\Sigma}$. The value of $\mathcal{Z}$ will then be obtained using the transformation of the time-harmonic solutions described in LEMMA 4 and the transformation of impedance-like coefficients described in THEOREM 6.

We will consider the Engquist-Madja absorbing boundary conditions, see [EM77], in the Lorentz variable.

We assume that the artificial boundary in Lorentz coordinates $\widetilde{\Sigma}$ is a circle of radius R.

ABC of order 0. The zeroth order ABC reads

$$\left(\partial_{\widetilde{\boldsymbol{n}}} - i\frac{\widetilde{\omega}}{c_0}\right)\widetilde{p} = 0.$$

The impedance-like operators are therefore defined by

$$\widetilde{\mathcal{Z}} := -i\frac{\widetilde{\omega}}{c_0} \quad \text{and} \quad \mathcal{Z} := i\left(\frac{c_0}{\alpha\mu} + \boldsymbol{v_0}\cdot\boldsymbol{n}\right)\omega. \tag{28}$$

It is now clear that ASSUMPTION 3 holds, so the ABC (28) leads to a well-posed problem. In the remaining of this paper, this ABC will be called ABC0.

ABC of order 1. The first order ABC reads

$$\left(\partial_{\widetilde{\boldsymbol{n}}} - i\frac{\widetilde{\omega}}{c_0} + \frac{1}{2R}\right)\widetilde{p} = 0.$$

The impedance-like operators are therefore defined by

$$\widetilde{\mathcal{Z}} := -i\frac{\widetilde{\omega}}{c_0} + \frac{1}{2R} \quad \text{and} \quad \mathcal{Z} := \frac{-c_0^2}{2\mu R} + i\left(\frac{c_0}{\alpha\mu} + \boldsymbol{v_0}\cdot\boldsymbol{n}\right)\omega. \tag{29}$$

Once again it is clear that ASSUMPTION 3 holds, so the ABC (29) also leads to a well-posed problem. In the remaining of this paper, this ABC will be called ABC1.

2.5.2. Plane-wave ABC

To dispose of comparison elements, we will derive an absorbing boundary condition on Σ by using a plane-wave analysis. This ABC will select outgoing plane-waves that are locally orthogonal to the artificial boundary Σ. In the remaining of this paper, it will be called ABC-PW.

We write

$$\boldsymbol{v_0} = Mc_0 \begin{bmatrix} \cos\theta_0 \\ \sin\theta_0 \end{bmatrix}, \theta_0 \in [0, 2\pi),$$

and

$$\boldsymbol{\kappa} = \kappa \begin{bmatrix} \cos\theta \\ \sin\theta \end{bmatrix}, \theta \in [0, 2\pi).$$

A direct computation shows that

$$\boldsymbol{\kappa}_\pm = \frac{\kappa_\pm}{Mc_0} \left(\cos(\theta - \theta_0)\boldsymbol{v_0} + \sin(\theta - \theta_0)\boldsymbol{v_0^\perp} \right).$$

Plane-wave solutions of (3) are

$$p = p_0 e^{i\boldsymbol{\kappa}_\pm \cdot \boldsymbol{x}}, \quad \text{with} \quad \kappa_\pm = \frac{\pm\omega}{c_0(1 \pm M\cos(\theta - \theta_0))},$$

see Appendix B. The total flux $\boldsymbol{\sigma}$ therefore satisfies

$$\boldsymbol{\sigma} = -i\frac{c_0\kappa_\pm}{M} \left((1 - M^2)\cos(\theta - \theta_0)\boldsymbol{v_0} + \sin(\theta - \theta_0)\boldsymbol{v_0^\perp} \right) p_0 e^{i\boldsymbol{\kappa}\cdot\boldsymbol{x}}.$$

For the artificial boundary Σ we have

$$\boldsymbol{n} = \frac{\boldsymbol{\kappa}_\pm}{|\boldsymbol{\kappa}_\pm|} = \begin{bmatrix} \cos\theta \\ \sin\theta \end{bmatrix},$$

leading to

$$\boldsymbol{v_0} \cdot \boldsymbol{n} = Mc_0\cos(\theta - \theta_0), \quad \text{and} \quad \boldsymbol{v_0^\perp} \cdot \boldsymbol{n} = Mc_0\sin(\theta - \theta_0).$$

We then have

$$\boldsymbol{\sigma} \cdot \boldsymbol{n} = -i\omega c_0 \left(1 \pm M\cos(\theta - \theta_0)\right) p = -i\omega \left(c_0 \pm \boldsymbol{v_0} \cdot \boldsymbol{n}\right) p.$$

We can now define the impedance-like operator $\mathcal{Z}$ as

$$\mathcal{Z} = \frac{-\boldsymbol{\sigma} \cdot \boldsymbol{n}}{p} = i\omega(c_0 + \boldsymbol{v_0} \cdot \boldsymbol{n}), \tag{30}$$

which leads to

$$\boldsymbol{\sigma} \cdot \boldsymbol{n} + i\omega(c_0 + \boldsymbol{v_0} \cdot \boldsymbol{n})p = 0.$$

We have chosen the ABC with the + sign as a consequence of the convention $e^{-i\omega t}$ that we use for time-harmonic solutions .

Once again Assumption 3 holds, so using this ABC leads to a well-posed problem.

3. Numerical experiments

The numerical experiments of this section will be performed using the HDG-$\boldsymbol{\sigma}$ method of [BRT21]. *Hybridizable Discontinuous Galerkin (HDG)* methods are mixed DG methods which rely on a static condensation process to obtain a reasonable numerical cost while keeping the advantages of DG methods. For a general introduction to those methods, we refer to [KSC12].

In this case, the following *first-order in space and second-order in frequency* formulation is used:

$$\begin{aligned} \boldsymbol{\sigma} + \boldsymbol{K_0}\nabla p + 2i\omega p \boldsymbol{v_0} &= 0, \\ -\omega^2 p + \operatorname{div}(\boldsymbol{\sigma}) &= s. \end{aligned}$$

As the *total flux* $\boldsymbol{\sigma}$ is an unknown of the method, it is very natural to work with the absorbing boundary condition (7).

This method has been implemented in the `hawen` solver, see [Fau21].

3.1. Experiments with a uniform flow

We consider a point-source in a uniform flow

$$\boldsymbol{M_0} := M \begin{bmatrix} \cos\theta_0 \\ \sin\theta_0 \end{bmatrix}, \quad s = \delta_{\mathbf{0}}, \quad c_0 = 1, \quad \omega = 6\pi.$$

Using Lemma 4 and standard theory on the Helmholtz equation we can express the reference solution as

$$\widetilde{p}_{\mathrm{ref}}(\widetilde{\boldsymbol{x}}, \widetilde{\omega}) = \frac{i}{4} H_0^{(1)}(\widetilde{\omega}\widetilde{r}),$$

which leads to

$$p_{\mathrm{ref}}(\boldsymbol{x}, \omega) = \frac{i}{4\alpha} H_0^{(1)}\left(\frac{\omega}{\alpha}|\boldsymbol{A}\boldsymbol{x}|\right) \exp\left(-\frac{i\omega}{\alpha^2 c_0}\boldsymbol{M_0}\cdot\boldsymbol{x}\right). \tag{31}$$

Unless stated otherwise, we will use $\theta_0 = \frac{\pi}{4}$ in this section as it leads to a circular artificial boundary in both physical and PGL coordinates. The effect of θ_0 will only be illustrated in the end of this section.

3.1.1. Validation of the ABCs

We define the relative error as

$$\mathcal{E}_{\mathcal{O}} := \sqrt{\frac{\sum_{K,i} |\mathfrak{Re}(p - p_{\mathrm{ref}})(\boldsymbol{x}_i^K)|^2}{\sum_{K,i} |\mathfrak{Re}(p_{\mathrm{ref}})(\boldsymbol{x}_i^K)|^2}},$$

where $(\boldsymbol{x}_i^K)_i$ are the degrees of freedom in element $K \in \mathcal{T}_h$. As the solution p_{ref} is singular at $\boldsymbol{x} = (0,0)$, the error will be computed on $\mathcal{O}\backslash B(\mathbf{0}, \rho)$ where $B(\mathbf{0}, \rho)$ is the open ball centered on $\boldsymbol{x} = \mathbf{0}$ with radius $\rho = 2h$.

Low Mach number. The relative error $\mathcal{E}_{\mathcal{O}}$ for various values of R is given in TABLE 1 for a low Mach number $M = 0.4$. In this case, we can see that the three ABCs perform well, even if the two PGL-based ABCs (ABC0 and ABC1) perform better than ABC-PW. As expected, ABC1 performs better than ABC0 and for $M = 0.4$, we can see that a relative error of $\sim 0.1\%$ is obtained even with $R = 0.5$.

R	ABC0 (28)	ABC1 (29)	ABC-PW (30)
0.5	3.49%	0.11%	4.69%
1.0	1.73%	0.15%	4.57%
1.5	1.16%	0.15%	3.89%
2.0	0.86%	0.14%	3.56%

Table 1: Relative error $\mathcal{E}_{\mathcal{O}}$ in the domain for $M = 0.4$

Intermediate Mach number. In TABLE 2, the relative error $\mathcal{E}_{\mathcal{O}}$ is computed for several values of R for $M = 0.6$. In this case ABC-PW performs badly, leading to an error level of $\sim 10\%$, whereas the PGL-based ABCs give good numerical results with an error level of $\sim 1\%$. This is also illustrated in FIGURE 3. Once again ABC1 performs better than ABC0. Indeed ABC1 leads to an error level below 1% even for very small values of R whereas a larger R is required to obtain a similar error level with ABC0.

R	ABC0 (28)	ABC1 (29)	ABC-PW (30)
0.5	3.20%	0.91%	10.14%
1.0	1.58%	0.82%	9.02%
1.5	1.17%	0.83%	9.60%
2.0	0.98%	0.75%	8.23%

Table 2: Relative error $\mathcal{E}_{\mathcal{O}}$ in the domain for $M = 0.6$

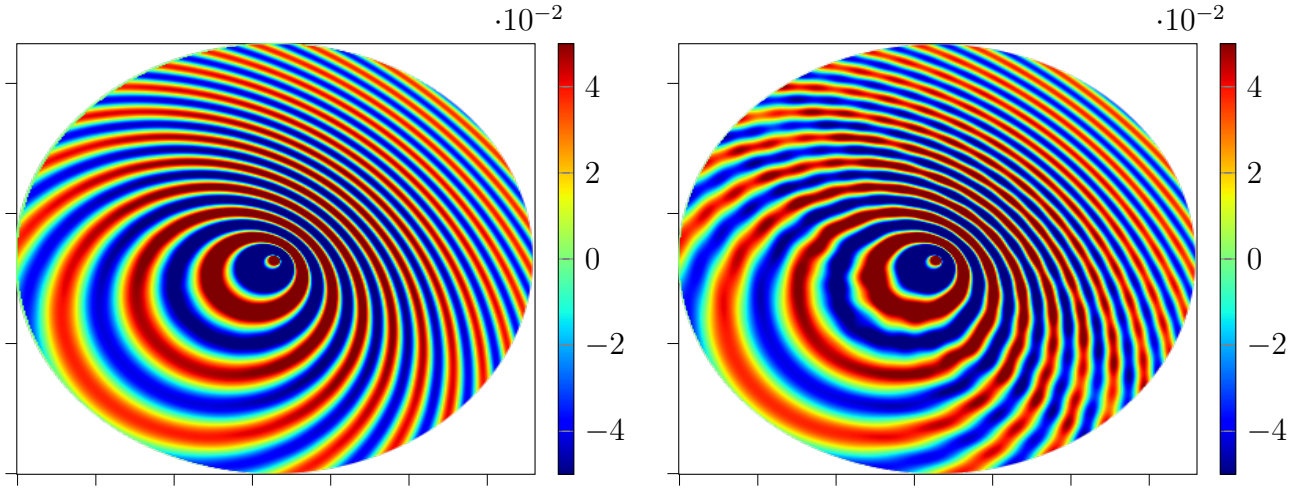

(a) ABC1 (b) ABC-PW

Figure 3: Comparison between two ABCs for $M = 0.6$ and $R = 2$

To understand the distribution of the error in the domain, we also consider the error in decibel (dB)

$$\mathcal{E}_{\mathrm{dB}} := 20 \log_{10} \left| \frac{p_h}{p_{\mathrm{ref}} + 10^{-12}} \right| .$$

Notice that we have added absolute values and a small term in the denominator to avoid invalid values due to floating-point arithmetic inside the logarithm.

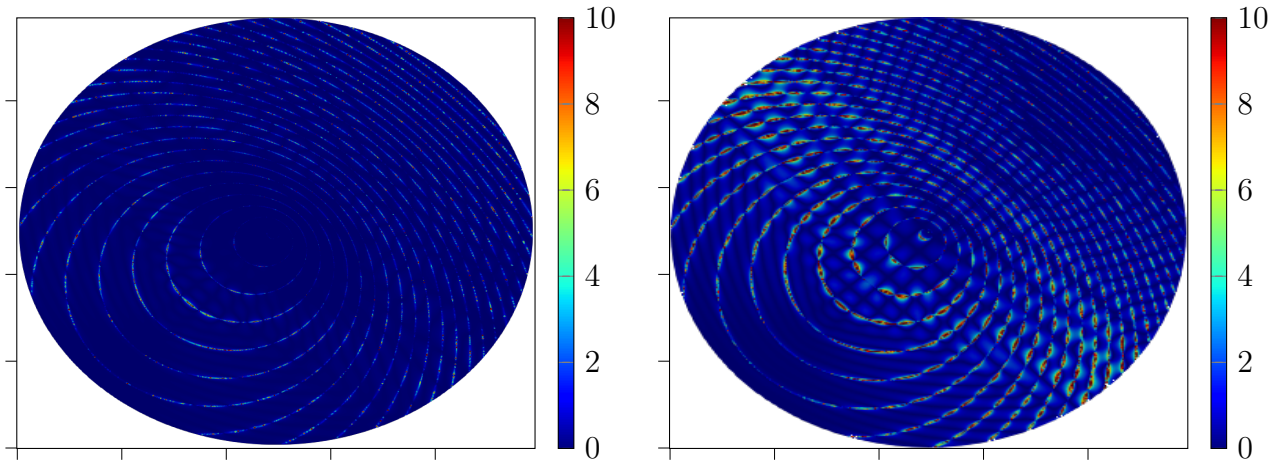

(a) ABC1 (b) ABC-PW

Figure 4: Error in dB $|\mathcal{E}_{\mathrm{dB}}|$ in the domain for $M = 0.6$ and $R = 2$

In FIGURE 4, the error in decibel in plotted for ABC1 and ABC-PW for $M = 0.6$ and $R = 2$. For ABC1, we cannot really see a pattern for the error distribution. For ABC-PW

however there is a clear pattern: the ABC performs better in the top-right and bottom-left parts of the domain. This can be understood as this ABC is constructed to select outgoing plane-waves that are locally orthogonal to the boundary. By looking at FIGURE 3, we can see that p is almost orthogonal to the boundary in the top-right and bottom-left parts of the domain where ABC-PW performs well. However due to the presence of convection, p is clearly not orthogonal to the boundary in the top-left and bottom-right parts of the domain, where ABC-PW exhibits its worst behavior.

To further illustrate this idea, we also consider the *local error* on the artificial boundary Σ

$$\mathcal{E}_\Sigma := |\mathfrak{Re}(p_h - p_{\text{ref}})|_\Sigma| \,.$$

This error is depicted in FIGURE 5 for ABC1 and ABC-PW. For ABC-PW, the same effect as in FIGURE 4 can be seen. For ABC1 however, we notice that most of the error is located in bottom part of the domain. We would like to point out that the error levels for ABC1 are one order of magnitude lower than those of ABC-PW as expected.

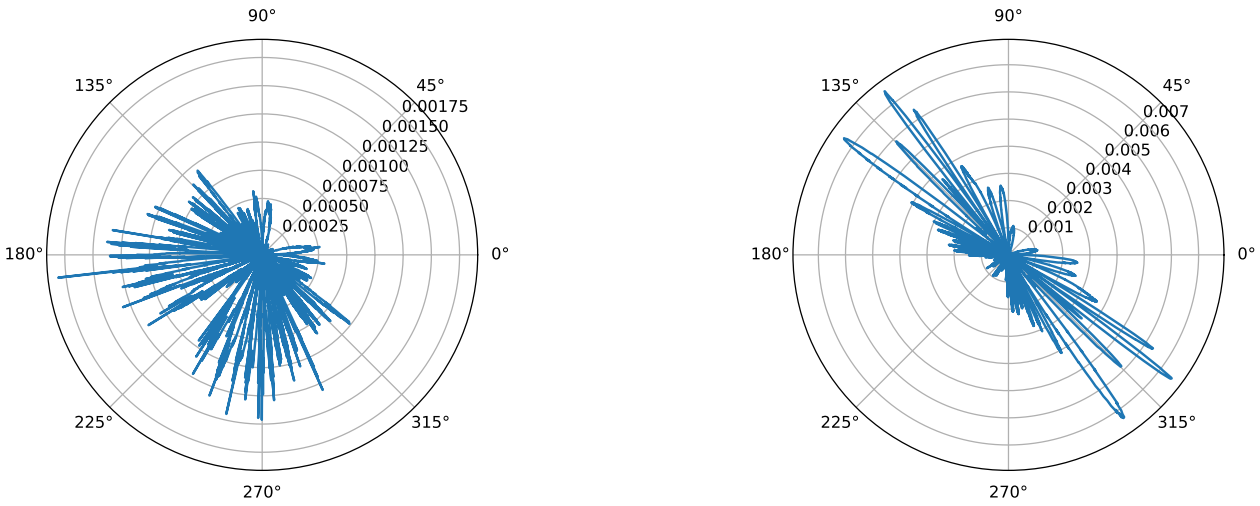

(a) ABC1 (b) ABC-PW

Figure 5: Local error $\mathcal{E}_\Sigma$ on Σ for $M = 0.6$ and $R = 2$

Large Mach number. For a large Mach number, the use of the PGL-based ABCs leads to a higher error. It therefore seems natural to consider larger domain, but as it can be seen in TABLE 3, even for $R = 10$ the error does not get below 2% with ABC1. It also seems that in this case, using ABC1 instead of ABC0 does not improve the quality of the solution.

R	ABC0 (28)	ABC1 (29)	ABC-PW (30)
3	2.71%	2.69%	16.92%
10	2.06%	2.05%	14.87%

Table 3: Relative error $\mathcal{E}_{\mathcal{O}}$ in the domain for $M = 0.8$

In FIGURE 6 we have plotted the numerical solution p_h obtained with ABC1 and ABC-PW for the smaller domain. Even if we can see some artifacts in the bottom-left part of the domain with ABC1, the quality of the result is clearly far superior than with ABC-PW.

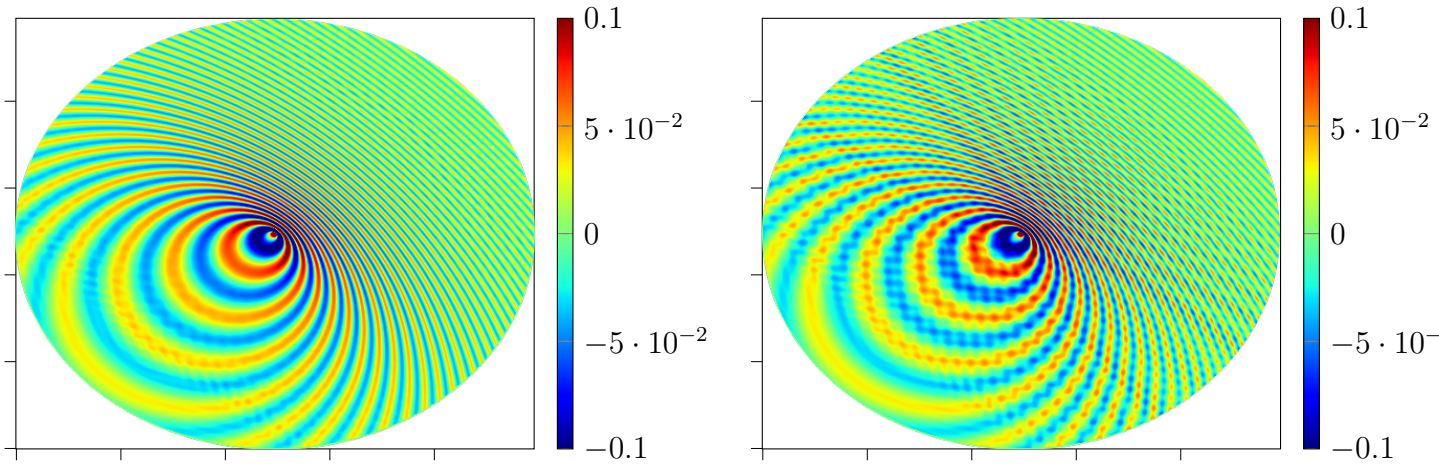

(a) ABC1 (b) ABC-PW

Figure 6: Comparison between two ABCs for $M = 0.8$ with $R = 3$

In FIGURE 7 we have depicted the numerical solution p_h and the error in decibel $\mathcal{E}_{\text{dB}}$ for ABC1 with $R = 10$. Even if the relative error $\mathcal{E}_{\mathcal{O}}$ is of 2.05%, by looking at the plot of $\mathcal{E}_{\text{dB}}$ it seems possible to trust the solution far enough from the artificial boundary.

Finally we would like to point out that considering a larger domain leads to a much more expensive problem from a computational point of view. The numerical experiments were runned on a `miriel` node of the `plafrim` cluster[1] equipped with 2 dodeca-core Haswell Intel Xeon E5-2680 v3 with a clock rate of 2.5 GHz and 128 Go of memory. The case in the small domain with $R = 3$ ran in 1min, whereas for the test with $R = 10$, it took 1h15min to run.

3.1.2. Influence of the flow angle

In this section, we try to understand the influence of the flow angle θ_0 on the performance of the ABCs. In TABLE 4 the errors obtained when using ABC1 are given for various values of θ_0. We can clearly see that $\mathcal{E}_{\mathcal{O}}$ is smaller when the flow is aligned with one of the axis (for $\theta_0 = 0$ or $\theta_0 = \pi/2$). This can be understood as the change of spatial coordinates $\boldsymbol{A}^{-1}$, which

[1] See `https://www.plafrim.fr`.

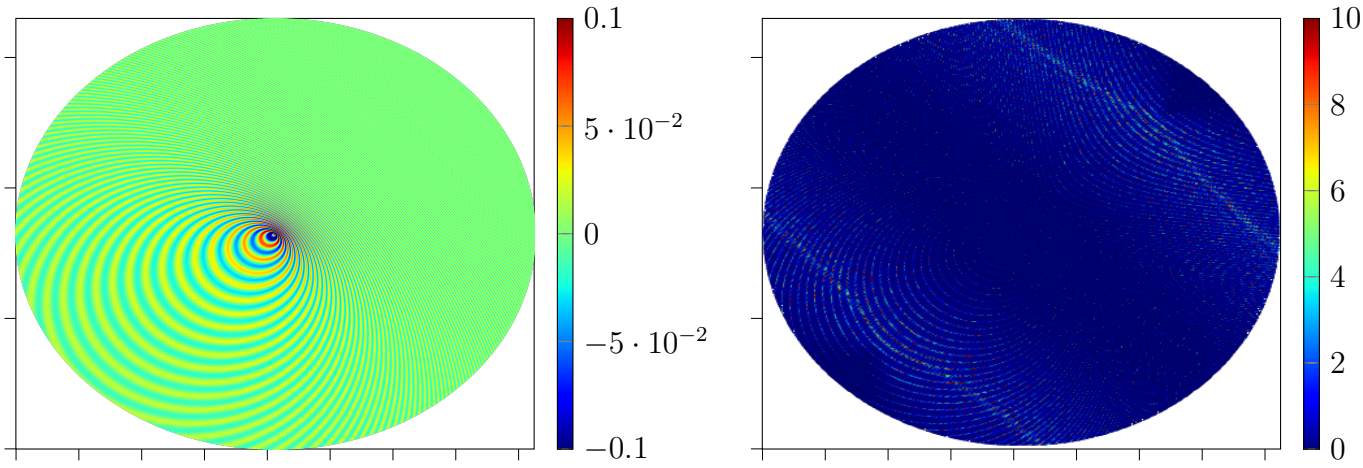

(a) Numerical solution p_h (b) $\mathcal{E}_{\text{dB}}$

Figure 7: Results and error for ABC1 with $M = 0.8$ and $R = 10$

is used to construct the ABCs, is contracting: the domain is smaller in physical coordinates than in PGL ones. When $\theta_0 = 0$ or $\pi/2$, this contraction only occurs in one direction, whereas it occurs in both directions for the other values of θ_0. The error is therefore smaller when the flow is aligned with one of the axis. The maximal error appears to be achieved for $\theta_0 = \pi/4$ which is the angle with the highest contraction, as both directions are contracted in the same way.

Flow angle θ_0	Error $\mathcal{E}_{\mathcal{O}}$
0	$1.38 \cdot 10^{-3}\%$
$\pi/3$	0.40%
$\pi/4$	0.65%
$\pi/6$	0.41%
$\pi/2$	$1.37 \cdot 10^{-3}\%$

Table 4: Domain error $\mathcal{E}_{\mathcal{O}}$ for $M = 0.6$ with ABC1 and $R = 2.5$

As the error seems minimal for a flow aligned with one of the axis, performing a rotation should therefore be considered before using those ABCs. However as the relative error stays below 1%, results obtained for other values of θ_0 are exploitable.

Some of the cases of Table 4 are depicted in Figure 8. On those figures, the elliptical shapes of the domain can clearly be seen when $\theta_0 \neq \pi/4$, as well as the contraction effect due to the change of coordinates.

3.1.3. Illustrative examples with multiple sources

To illustrate the ability of the ABCs to handle more complex cases, we consider multiple point-sources in a uniform flow. For the numerical simulations, the following parameters are

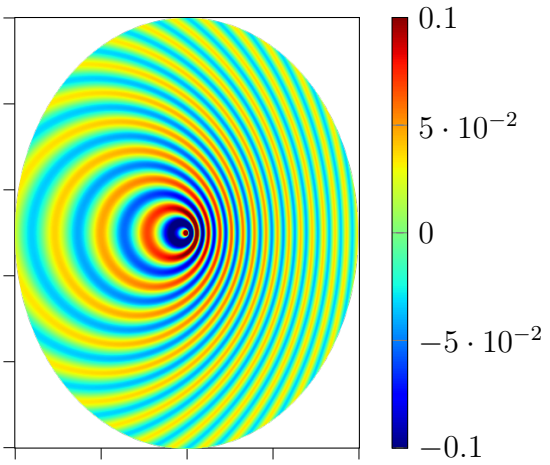

(a) $\theta_0 = 0$

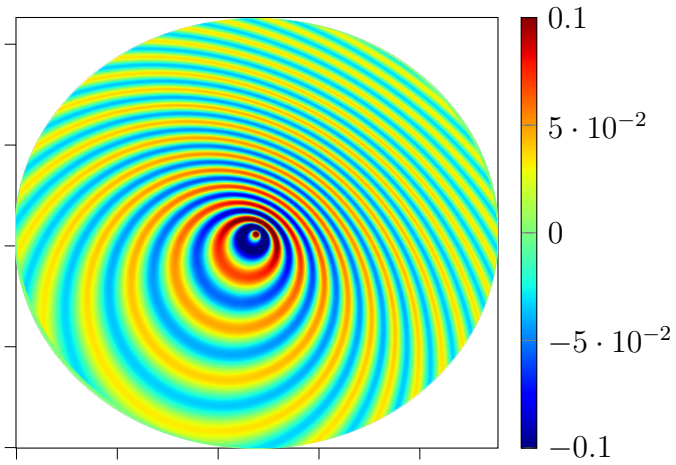

(b) $\theta_0 = \frac{\pi}{3}$

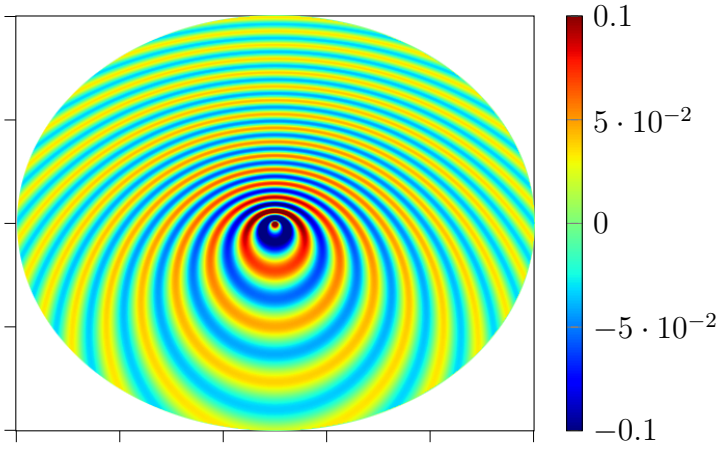

(c) $\theta_0 = \frac{\pi}{2}$

Figure 8: Numerical examples for various values of θ_0 with $M = 0.6$ and ABC1

used

$$M = 0.6, \quad \theta_0 = \frac{\pi}{4}, \quad \omega = 6\pi, \quad R = 2.$$

The sources will be located at $(\pm 0.1, \pm 0.1)$ for the case with two point-sources and at $(\pm 0.1, \pm 0.1)$ and $(\pm 0.1, \mp 0.1)$ for the case with four point-sources.

In FIGURE 9 the results obtained with the above parameters and ABC1 are depicted. We can clearly see the interference patterns between the sources as well as changes in the apparent frequency due to the Doppler effect. Those physical phenomena seem to be handled well by the ABC and it looks like there is no numerical pollution inside the domain

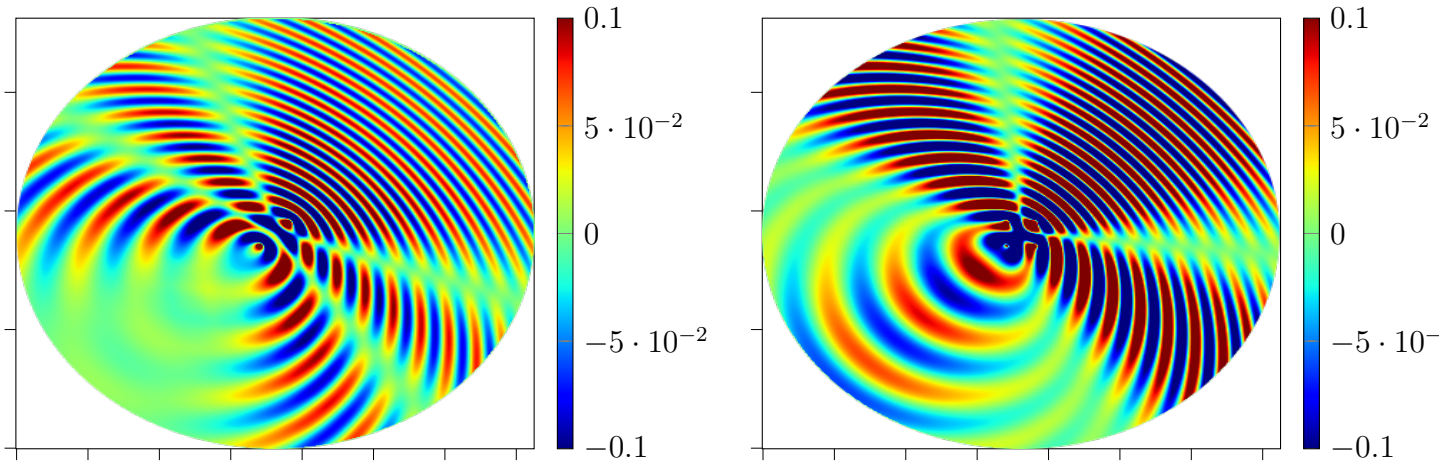

(a) Two point-sources

(b) Four point-sources

Figure 9: Interferences between multiple point-sources for $M = 0.6$ with ABC1

3.2. Experiments with a potential flow

In this section, we give illustrative examples where the PGL-based ABCs are used with a non-uniform flow. As the convected Helmholtz equation is only valid for potential flows, we focus on the case of a potential flow around a circular obstacle.

The ABCs of this paper are constructed for an artificial boundary Σ centered on the source. The expression for the potential flow should therefore be translated as it is usually written for a circular obstacle located at $(0, 0)$.

We assume that the obstacle has a radius of R_C and its center is located at $\boldsymbol{x}_C = (x_C, y_C)$. For a point $\boldsymbol{x} = (x, y)$, we define the translated polar coordinates around $\boldsymbol{x}_C$ by

$$r := |\boldsymbol{x} - \boldsymbol{x}_C|, \quad \text{and} \quad \theta := \arctan\left(\frac{y - y_C}{x - x_C}\right).$$

Let M_∞ be the Mach number of the flow at infinity, the potential flow is naturally expressed in the previous polar coordinates by

$$\boldsymbol{v_0} := M_\infty \left[\left(1 - \frac{R_C^2}{r^2}\right)\cos\theta \boldsymbol{e}_r - \left(1 + \frac{R_C^2}{r^2}\right)\sin\theta \boldsymbol{e}_\theta\right],$$

leading to the following expression in cartesian coordinates

$$\boldsymbol{v_0} = M_\infty \Big[\left(\frac{x - x_C}{r} \left(1 - \frac{R_C^2}{r^2} \right) \cos\theta + \frac{y - y_C}{r} \left(1 + \frac{R_C^2}{r^2} \right) \sin\theta \right) \boldsymbol{e}_x + \left(\frac{y - y_C}{r} \left(1 - \frac{R_C^2}{r^2} \right) \cos\theta - \frac{x - x_C}{r} \left(1 + \frac{R_C^2}{r^2} \right) \sin\theta \right) \boldsymbol{e}_y \Big].$$

The configuration for this case is depicted in FIGURE 10.

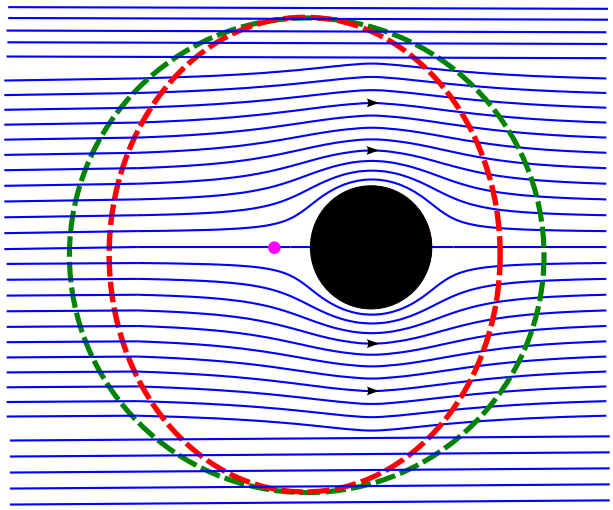

Figure 10: Sketch of the settings: in blue: streamlines of $\boldsymbol{v_0}$, in red: artificial boundary Σ, in green: artificial boundary in PGL coordinates, in magenta: point-source, in black: obstacle

In FIGURE 11, we depicted p_h obtained with the following parameters

$$\boldsymbol{x}_C = (\pm 1, 0), \quad R_C = 0.5, \quad M_\infty = 0.4, \quad \omega = 6\pi.$$

It seems there is no reflection at the artificial boundary Σ and the expected physical phenomena are visible. We can clearly see a change in apparent frequency due to the Doppler effect, phase-shifts due to a refraction-like effect and an interference pattern due to the reflection of the wave on the obstacle. For the upstream example, we can also see a silent zone behind the obstacle as expected. For the downstream case, creeping waves can be seen around the obstacle, and a constructive interference pattern is visible behind the obstacle.

Similar cases to the upstream one have been studied in [BCD+14], the differences between the results obtained by the authors and our results may be explained by a different kind of source term and differences between 2D and 3D simulations. In particular, the pressure inside the silent cone is lower in our results.

Similar cases to the downstream one have been considered in [LMG+20]. The results obtained by the authors are very similar to the ones of this paper, therefore validating the new ABCs that we have constructed.

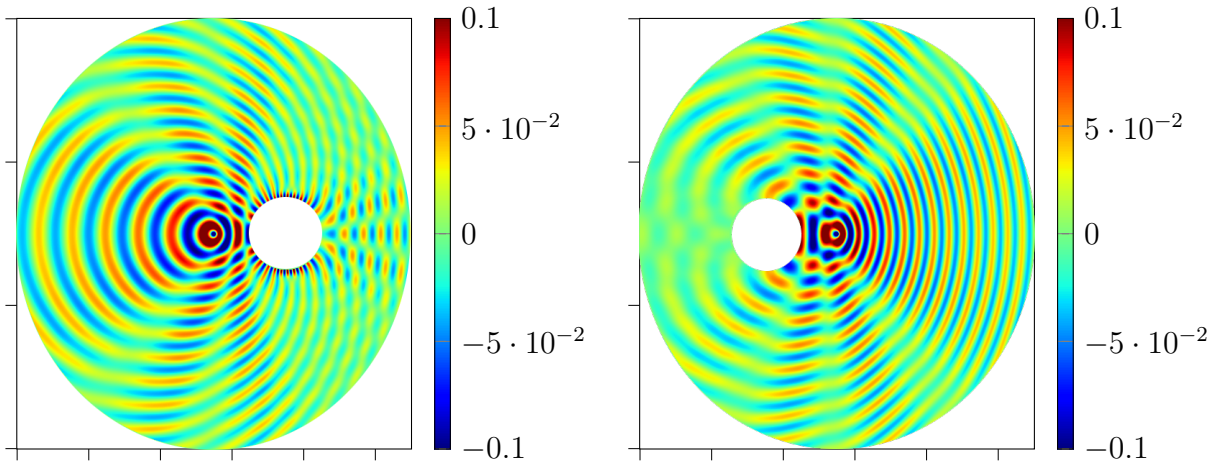

(a) Downstream obstacle

(b) Upstream obstacle

Figure 11: Point-source in a potential flow around a circular obstacle for $M_\infty = 0.4$

Conclusion

In this paper, we have seen that the use of the *Prandtl-Glauert-Lorentz transformation* to construct ABCs for the convected Helmholtz equation leads to very good results for low and intermediate Mach numbers. For higher Mach numbers, a very large domain seems to be required and the ABCs constructed in this paper should be used carefully. Due to the presence of convection, the usual idea of selecting waves that are locally orthogonal to the boundary leads to bad results, and the PGL-based ABCs should be preferred. Among those ABCs, the use of ABC1 instead of ABC0 gives better results for no additional cost. Finally we would like to point out that the ABCs constructed in this paper are really easy to implement in an existing finite-element solver for the convected Helmholtz equation as the PGL transformation is only required to compute the impedance-like operator $\mathcal{Z}$.

In [Gab03, Chap. 3] and [Bér08, Chap. 5], ABCs for Galbrun's equation are studied. Galbrun's equation is an aeroacoustic model which is more realistic than the convected Helmholtz equation as it allows for more general background flows. However the ABCs derived in those dissertations were only illustrated with uniform flows for which the two models are equivalent. This can clearly be seen as the reference solution used in [Bér08, p. 129 - last equation] is the same as the one we described in (31). Even if various conditions are described, the best performing one is somewhat similar to the ABC-PW condition (30) of this paper, and the authors only obtained an error level of 4.5% for $M = 0.3$ and $\omega = 6\pi$.

For the convected Helmholtz equation, usual PMLs are known to be unstable. In [BBL03] stable PMLs for the convected Helmholtz equation were derived, but only for propagation in a waveguide. This work was extended to arbitrary geometries in [MBAG20], this formulation is also based on the *Prandtl-Glauert-Lorentz transformation*. For high Mach numbers, the so-called Lorentz PMLs of [MBAG20] seem to perform better than the ABCs of this paper.

Indeed, the authors were able to obtain an error level fo 1.2% using a smaller domain for $M = 0.8$. However this formulation seems difficult to implement in the context of HDG methods and, as stated in [MAGB21], their efficiency for non-uniform flows remains unclear. Finally, we would like to point out that similar PMLs have been derived for time-domain convected acoustic wave equation in [DJ06].

Perspectives. Even if we only presented 2D results, the extension of this work to 3D is straightforward as the result of Theorem 6 relating $\mathcal{Z}$ and $\widetilde{\mathcal{Z}}$ holds for any dimension.

Extension of this work to higher order boundary conditions is possible even if the expected gain is not clear. Indeed the new ABCs are based on ABCs for the standard Helmholtz equation on a circle, and as pointed out in [ABB99] there is no real benefit in using higher-order ABCs in this case.

Extension to more realistic aeroacoustic models seem possible. The most straightforward model to consider for this extension is Goldstein's equation [MMMP17] which consists in a coupling between a convected Helmholtz equation and a vectorial transport equation. The ABCs of this paper could be used for the convected Helmholtz equation and it is possible to obtain an exact outgoing condition for the transport equation. Extension to Galbrun's equation [BMM+12] or to the Linearized Euler's Equations [BBJ02] seems more complicated, mostly due to the lack of a "standard" equation for which ABCs can be derived.

Acknowledgement

The authors would like to thank Florian Faucher for his help with the numerical implementation.

Experiments presented in this paper were carried out using the PlaFRIM experimental testbed, supported by Inria, CNRS (LABRI and IMB), Université de Bordeaux, Bordeaux INP and Conseil Régional d'Aquitaine (see https://www.plafrim.fr).

Funding

Nathan Rouxelin was supported by a grant from e2s-UPPA (see https://e2s-uppa.eu).

Appendix A. Proof of Lemma 7

In this appendix, we prove the result of Lemma 7. As the numerical examples of this paper are in 2D, we have chosen to prove the result in the same dimension. Extension to 3D is straightforward and would involve the standard 3D Green functions instead of the Hankel functions.

PROOF. This result is proven by using the *limiting amplitude principle* which consists in studying the long-term behaviour of the time-domain solution with the following source term

$$g(\boldsymbol{x},t) = \begin{cases} s(\boldsymbol{x})e^{-i\omega t}, & \text{if } t > 0 \\ 0, & \text{if } t \leqslant 0 \end{cases},$$

where s is a function in $L^2(\mathcal{O})$ with compact support.

Step 1: Green functions in time-domain.
The Green function for the two-dimensional acoustic wave-equation in time-domain reads

$$G_{\text{std}}(\boldsymbol{x},t) = \frac{H\left(t - \frac{r}{c_0}\right)}{2\pi\sqrt{t^2 - \frac{r^2}{c_0^2}}},$$

where H is the Heaviside function and $r = |\boldsymbol{x}|$. For the proof, we refer to [DJ06, Th. 1] or [Ver10, Sec. A.4.2].

The Green function for the convected wave equation in time-domain has been computed in the case $\boldsymbol{M_0} = M\boldsymbol{e}_x$ using the *Cagniard-de Hoop method* in [DJ06, Th. 6]. The case of a generic $\boldsymbol{M_0}$ reduces to this one by rotation. In this paper, the parameter σ denotes the absorption parameter used in PMLs, so we take $\sigma = 0$ leading to $A = B = 0$.

With the assumption that $\boldsymbol{M_0} = M\boldsymbol{e}_x$, the *Prandtl-Glauert-Lorentz transformation* reads

$$\widetilde{t} = \alpha t + \frac{1}{\alpha c_0} Mx, \quad \widetilde{x} = \frac{x}{\alpha}, \quad \widetilde{y} = y, \quad \widetilde{r}^2 = \widetilde{x}^2 + \widetilde{y}^2, \quad \widetilde{\theta} = \arctan\frac{\widetilde{y}}{\widetilde{x}}. \tag{A.1}$$

We define the following change of variables in space

$$\hat{x} = \frac{\widetilde{x}}{\alpha}, \quad \text{and} \quad \hat{y} = \frac{\widetilde{y}}{\alpha}. \tag{A.2a}$$

In polar coordinates, we also define

$$\hat{r}^2 = \hat{x}^2 + \hat{y}^2, \quad \text{and} \quad \hat{\theta} = \arctan\frac{\hat{y}}{\hat{x}}. \tag{A.2b}$$

It is straightforward to check that

$$\hat{r} = \frac{\widetilde{r}}{\alpha}, \quad \text{and} \quad \hat{\theta} = \widetilde{\theta}.$$

The Green function corresponding to the convected acoustic wave equation reads

$$G_{\text{conv}}(\boldsymbol{x},t) = \frac{H(t - \frac{\hat{r}}{c_0}(1 - M\cos\hat{\theta}))}{2\pi\sqrt{1-M^2}\sqrt{(t + \frac{M\hat{r}}{c_0}\cos\hat{\theta})^2 - \frac{\hat{r}^2}{c_0}}}.$$

Using the intermediate change of variables (A.2a)–(A.2b) and expressing in terms of the *Prandt-Glauert-Lorentz coordinates* (A.1), we have

$$\begin{aligned}
G_{\text{conv}}(\boldsymbol{x},t) &= \frac{H\left(t+\frac{M}{c_0}\hat{x}-\frac{\hat{r}}{c_0}\right)}{2\pi\alpha\sqrt{(t+\frac{M}{c_0}\hat{x})^2-\frac{\hat{r}^2}{c_0^2}}},\\
&= \frac{H\left(t+\frac{M}{\alpha c_0}\widetilde{x}-\frac{\widetilde{r}}{\alpha c_0}\right)}{2\pi\alpha\sqrt{(t+\frac{M}{\alpha c_0}\widetilde{x})^2-\frac{\widetilde{r}^2}{\alpha^2 c_0^2}}},\\
&= \frac{H\left(t+\frac{M}{\alpha^2 c_0}x-\frac{\widetilde{r}}{\alpha c_0}\right)}{2\pi\alpha\sqrt{(t+\frac{M}{\alpha^2 c_0}x)^2-\frac{\widetilde{r}^2}{\alpha^2 c_0^2}}},\\
&= \frac{H\left(\frac{1}{\alpha}\left[\alpha t+\frac{M}{\alpha c_0}x-\frac{\widetilde{r}}{c_0}\right]\right)}{2\pi\alpha\frac{1}{\alpha}\sqrt{(\alpha t+\frac{M}{\alpha c_0}x)^2-\frac{\widetilde{r}^2}{c_0^2}}},\\
&= \frac{H\left(\widetilde{t}-\frac{\widetilde{r}}{c_0}\right)}{2\pi\sqrt{\widetilde{t}^2-\frac{\widetilde{r}^2}{c_0^2}}}\\
&= G_{\text{std}}(\widetilde{\boldsymbol{x}},\widetilde{t}).
\end{aligned}$$

As G_{conv} is mapped to G_{std} through the *Prandtl-Glauert-Lorentz transformation*, we can therefore prove that this transform also maps outgoing solutions to outgoing solutions by using standard arguments of the *limiting amplitude principle*.

Step 2: Limiting amplitude principle for the standard Helmholtz equation.

We recall that the following identities hold

$$\int_r^{+\infty}\frac{e^{i\omega t}}{2\pi\sqrt{t^2-r^2}}\mathrm{d}t=\frac{1}{2\pi}\int_0^{+\infty}e^{i\omega r\cosh\theta}\mathrm{d}\theta=\frac{i}{4}H_0^{(1)}(\omega r), \tag{A.3}$$

where used the following change of variables $t=r\cosh\theta$ and the integral form of the Hankel function, see [OLBC10, Eq. 10.9.10].

Using the integral representation we have

$$p_{\text{std}}(\boldsymbol{x},t)=\int_{\mathbb{R}^2}\int_{\mathbb{R}}G_{\text{std}}(\boldsymbol{x}_1,t_1)g(\boldsymbol{x}-\boldsymbol{x}_1,t-t_1)\mathrm{d}t_1\mathrm{d}\boldsymbol{x}_1,$$

using the integral identity (A.3) for the Hanekl function, we have

$$=\int_{\mathbb{R}^2}\int_{\frac{|\boldsymbol{x}_1|}{c_0}}^{+\infty}\frac{g(\boldsymbol{x}-\boldsymbol{x}_1,t-t_1)}{2\pi\sqrt{t_1^2-\frac{|\boldsymbol{x}_1|^2}{c_0^2}}}\mathrm{d}t_1\mathrm{d}\boldsymbol{x}_1$$

using that $g(\boldsymbol{x},t) = s(\boldsymbol{x})e^{-i\omega t}H(t)$, where s is a L^2-function with compact support,

$$\begin{aligned}
&= \int_{\mathbb{R}^2} s(\boldsymbol{x}-\boldsymbol{x}_1)e^{-i\omega t}\int_{\frac{|\boldsymbol{x}_1|}{c_0}}^{t} \frac{e^{i\omega t_1}}{2\pi\sqrt{t_1^2-\frac{|\boldsymbol{x}_1|^2}{c_0^2}}}\mathrm{d}t_1\mathrm{d}\boldsymbol{x}_1\\
&= \int_{\mathbb{R}^2} s(\boldsymbol{x}-\boldsymbol{x}_1)e^{-i\omega t}\left[\frac{i}{4}H_0^{(1)}\left(\frac{\omega}{c_0}|\boldsymbol{x}_1|\right)+\mathfrak{r}_{\mathrm{std}}\right]\mathrm{d}\boldsymbol{x}_1
\end{aligned}$$

where $\mathfrak{r}_{\mathrm{std}}(\boldsymbol{x}_1,t) = -\int_t^{+\infty}\frac{e^{i\omega t_1}}{2\pi\sqrt{t_1^2-\frac{|\boldsymbol{x}_1|^2}{c_0^2}}}\mathrm{d}t_1$ with $t > \frac{|\boldsymbol{x}_1|}{c_0}$,

$$= \int_{\mathbb{R}^2} s(\boldsymbol{x}-\boldsymbol{x}_1)e^{-i\omega t}\frac{i}{4}H_0^{(1)}\left(\frac{\omega}{c_0}|\boldsymbol{x}_1|\right)\mathrm{d}\boldsymbol{x}_1 + \mathfrak{R}_{\mathrm{std}},$$

and

$$\mathfrak{R}_{\mathrm{std}}(\boldsymbol{x},t) = e^{-i\omega t}\int_{\mathbb{R}^2} s(\boldsymbol{x}-\boldsymbol{x}_1)\mathfrak{r}_{\mathrm{std}}(\boldsymbol{x}_1,t)\mathrm{d}\boldsymbol{x}_1 = -e^{-i\omega t}\int_{\mathbb{R}^2} s(\boldsymbol{x}-\boldsymbol{x}_1)\int_t^{+\infty}\frac{e^{i\omega t_1}}{2\pi\sqrt{t_1^2-\frac{|\boldsymbol{x}_1|^2}{c_0^2}}}\mathrm{d}t_1\mathrm{d}\boldsymbol{x}_1.$$

We now prove that $\mathfrak{R}_{\mathrm{std}}(\boldsymbol{x},t) \xrightarrow[t\to+\infty]{} 0$. The first step is to show that the integral defining $\mathfrak{r}_{\mathrm{std}}$ is actually finite-valued. We have

$$\begin{aligned}
\mathfrak{r}_{\mathrm{std}}(\boldsymbol{x}_1,t) &:= -\int_t^{+\infty}\frac{e^{i\omega t_1}}{2\pi\sqrt{t_1^2-\frac{|\boldsymbol{x}_1|^2}{c_0^2}}}\mathrm{d}t_1\\
&= -\lim_{A\to+\infty}\left(\left[\frac{e^{i\omega t_1}}{2i\pi\omega\sqrt{t_1^2-\frac{|\boldsymbol{x}_1|^2}{c_0^2}}}\right]_t^A + \int_t^A \frac{t_1 e^{i\omega t_1}}{2\pi\left(t_1^2-\frac{|\boldsymbol{x}_1|^2}{c_0^2}\right)^{\frac{3}{2}}}\mathrm{d}t_1\right)\\
&< +\infty,
\end{aligned}$$

as

$$\lim_{A\to+\infty}\frac{e^{i\omega A}}{2i\pi\omega\sqrt{A^2-\frac{|\boldsymbol{x}_1|^2}{c_0^2}}} = 0, \quad \text{and} \quad \left|\frac{t_1 e^{i\omega t_1}}{2\pi\left(t_1^2-\frac{|\boldsymbol{x}_1|^2}{c_0^2}\right)^{\frac{3}{2}}}\right| = \frac{t_1}{2\pi\left(t_1^2-\frac{|\boldsymbol{x}_1|^2}{c_0^2}\right)^{\frac{3}{2}}} \underset{t_1\to\infty}{\sim} \frac{1}{t_1^2}.$$

We can therefore express $\mathfrak{r}_{\mathrm{std}}$ as

$$\mathfrak{r}_{\mathrm{std}}(\boldsymbol{x}_1,t) = -\frac{e^{i\omega t}}{2i\pi\omega\sqrt{t^2-\frac{|\boldsymbol{x}_1|^2}{c_0^2}}} - \int_t^{+\infty}\frac{t_1 e^{i\omega t_1}}{2\pi\left(t_1^2-\frac{|\boldsymbol{x}_1|^2}{c_0^2}\right)^{\frac{3}{2}}}\mathrm{d}t_1$$

and $\mathfrak{R}_{\mathrm{std}}$ as

$$\mathfrak{R}_{\mathrm{std}}(\boldsymbol{x},t) = \int_{\mathbb{R}^2}\frac{s(\boldsymbol{x}-\boldsymbol{x}_1)}{2\pi\sqrt{t^2-\frac{|\boldsymbol{x}_1|^2}{c_0^2}}}\mathrm{d}\boldsymbol{x}_1 + e^{-i\omega t}\int_{\mathbb{R}^2} s(\boldsymbol{x}-\boldsymbol{x}_1)\int_t^{+\infty}\frac{t_1 e^{i\omega t_1}}{2\pi\left(t_1^2-\frac{|\boldsymbol{x}_1|^2}{c_0^2}\right)^{\frac{3}{2}}}\mathrm{d}t_1\mathrm{d}\boldsymbol{x}_1.$$

We can now show that both of these quantities vanish at infinity. Let us first focus on the first term in $\mathfrak{R}_{\text{std}}$

$$\int_{\mathbb{R}^2} \frac{s(\boldsymbol{x}-\boldsymbol{x}_1)}{2\pi\sqrt{t^2-\frac{|\boldsymbol{x}_1|^2}{c_0^2}}}\mathrm{d}\boldsymbol{x}_1.$$

As we are interested in the limit as $t \to +\infty$ and as the space integral is over a compact domain, we can assume that

$$\frac{3t^2}{4} > \frac{|\boldsymbol{x}_1|^2}{c_0^2},$$

which leads to

$$\frac{|s(\boldsymbol{x}-\boldsymbol{x}_1)|}{2\pi\sqrt{t^2-\frac{|\boldsymbol{x}_1|^2}{c_0^2}}} < \frac{|s(\boldsymbol{x}-\boldsymbol{x}_1)|}{\pi|t|},$$

and we have

$$\int_{\mathbb{R}^2} \left|\frac{s(\boldsymbol{x}-\boldsymbol{x}_1)}{2\pi\sqrt{t^2-\frac{|\boldsymbol{x}_1|^2}{c_0^2}}}\right| \mathrm{d}\boldsymbol{x}_1 \leqslant \frac{1}{\pi|t|}\int_{\mathbb{R}^2} |s(\boldsymbol{x}-\boldsymbol{x}_1)|\mathrm{d}\boldsymbol{x}_1 \xrightarrow[t\to+\infty]{} 0,$$

as the last integral is over a compact domain. By taking the limit in the previous inequality, we have

$$\lim_{t\to+\infty}\int_{\mathbb{R}^2} \left|\frac{s(\boldsymbol{x}-\boldsymbol{x}_1)}{2\pi\sqrt{t^2-\frac{|\boldsymbol{x}_1|^2}{c_0^2}}}\right| \mathrm{d}\boldsymbol{x}_1 = 0.$$

We can now work on the second term.

As we are interested in the limit as $t \to +\infty$ and as the space integral is over a compact domain, we can assume once again that

$$\frac{3t_1^2}{4} > \frac{3t^2}{4} > \frac{|\boldsymbol{x}_1|^2}{c_0^2},$$

which leads to

$$\frac{t_1}{2\pi\left(t_1^2-\frac{|\boldsymbol{x}_1|^2}{c_0^2}\right)^{\frac{3}{2}}} < \frac{t_1}{\frac{\pi}{4}t_1^3} = \frac{4}{\pi t_1^2}.$$

We therefore have

$$\int_t^{+\infty} \left|\frac{t_1 e^{i\omega t_1}}{2\pi\left(t_1^2-\frac{|\boldsymbol{x}_1|^2}{c_0^2}\right)^{\frac{3}{2}}}\right| \mathrm{d}t_1 < \frac{4}{\pi}\int_t^{+\infty}\frac{1}{t_1^2}\mathrm{d}t_1 = \frac{4}{\pi t} \xrightarrow[t\to+\infty]{} 0.$$

Finally we have

$$\int_{\mathbb{R}^2} |s(\boldsymbol{x}-\boldsymbol{x}_1)| \int_t^{+\infty} \left| \frac{t_1 e^{i\omega t_1}}{2\pi \left(t_1^2 - \frac{|\boldsymbol{x}_1|^2}{c_0^2}\right)^{\frac{3}{2}}} \right| \mathrm{d}t_1 \mathrm{d}\boldsymbol{x}_1 \leqslant \int_{\mathbb{R}^2} |s(\boldsymbol{x}-\boldsymbol{x}_1)| \frac{4}{\pi t} \mathrm{d}\boldsymbol{x}_1$$
$$\leqslant \frac{4}{\pi t} \int_{\mathbb{R}^2} |s(\boldsymbol{x}-\boldsymbol{x}_1)| \mathrm{d}\boldsymbol{x}_1 \xrightarrow[t\to+\infty]{} 0.$$

Notice that the last integral is finite as the support of s is compact. By taking the limit in the previous inequalities, we have

$$\lim_{t\to+\infty} \int_{\mathbb{R}^2} |s(\boldsymbol{x}-\boldsymbol{x}_1)| \int_t^{+\infty} \left| \frac{t_1 e^{i\omega t_1}}{2\pi \left(t_1^2 - \frac{|\boldsymbol{x}_1|^2}{c_0^2}\right)^{\frac{3}{2}}} \right| \mathrm{d}t_1 \mathrm{d}\boldsymbol{x}_1 = 0.$$

We therefore have

$$\lim_{t\to+\infty} |\mathfrak{R}_{\mathrm{std}}(\boldsymbol{x},t)| = 0, \quad \forall \boldsymbol{x} \in \mathbb{R}^2.$$

Now, we define the time-harmonic Green function by

$$W_{\mathrm{std}}(\boldsymbol{x},\omega) = \frac{i}{4} H_0^{(1)}\left(\frac{\omega}{c_0}|\boldsymbol{x}|\right).$$

We end up with the *limiting amplitude principle*

$$\lim_{t\to\infty} \left\| p_{\mathrm{std}}(\boldsymbol{x},t) - p_{\mathrm{std},\omega}(\boldsymbol{x}) e^{-i\omega t} \right\| = 0,$$

where $p_{\mathrm{std},\omega} := W_{\mathrm{std}}(\cdot,\omega) * s$ is the outgoing solution of the standard Helmholtz equation.

Step 3: Limiting amplitude principle for the convected Helmholtz equation. We have

$$\begin{aligned} p(\boldsymbol{x},t) &= \int_{\mathbb{R}^2} \int_{\mathbb{R}} G_{\mathrm{conv}}(\boldsymbol{x}_1,t_1) g(\boldsymbol{x}-\boldsymbol{x}_1, t-t_1) \mathrm{d}t_1 \mathrm{d}\boldsymbol{x}_1 \\ &= \int_{\mathbb{R}^2} \int_{\mathbb{R}} G_{\mathrm{std}}(\widetilde{\boldsymbol{x}}_1,\widetilde{t}_1) g\left(\boldsymbol{A}^{-1}(\widetilde{\boldsymbol{x}}-\widetilde{\boldsymbol{x}}_1), \frac{1}{\alpha}(\widetilde{t}-\widetilde{t}_1) + \frac{1}{\alpha c_0} \boldsymbol{M_0}\cdot(\widetilde{\boldsymbol{x}}-\widetilde{\boldsymbol{x}}_1)\right) \mathrm{d}\widetilde{t}_1 \mathrm{d}\widetilde{\boldsymbol{x}}_1 \\ &= \int_{\mathbb{R}^2} \int_{\frac{|\widetilde{\boldsymbol{x}}_1|}{c_0}}^{+\infty} \frac{g\left(\boldsymbol{A}^{-1}(\widetilde{\boldsymbol{x}}-\widetilde{\boldsymbol{x}}_1), \frac{1}{\alpha}(\widetilde{t}-\widetilde{t}_1) - \frac{1}{\alpha c_0}\boldsymbol{M_0}\cdot(\widetilde{\boldsymbol{x}}-\widetilde{\boldsymbol{x}}_1)\right)}{2\pi\sqrt{\widetilde{t}_1^2 - \frac{|\widetilde{\boldsymbol{x}}_1|^2}{c_0^2}}} \mathrm{d}\widetilde{t}_1 \mathrm{d}\widetilde{\boldsymbol{x}}_1 \end{aligned}$$

using that $g(\boldsymbol{x},t) = s(\boldsymbol{x}) e^{-i\omega t} H(t)$, where s is a function with compact support,

$$= \int_{\mathbb{R}^2} s(\boldsymbol{A}^{-1}(\widetilde{\boldsymbol{x}}-\widetilde{\boldsymbol{x}}_1)) e^{-i\omega(\frac{1}{\alpha}\widetilde{t} - \frac{1}{\alpha c_0}\boldsymbol{M_0}\cdot\widetilde{\boldsymbol{x}})} e^{-i\frac{\omega}{\alpha c_0}\boldsymbol{M_0}\cdot\widetilde{\boldsymbol{x}}_1} \int_{\frac{|\widetilde{\boldsymbol{x}}_1|}{c_0}}^{\widetilde{t}-\frac{\boldsymbol{M_0}}{c_0}\cdot(\widetilde{\boldsymbol{x}}-\widetilde{\boldsymbol{x}}_1)} \frac{e^{i\frac{\omega}{\alpha}\widetilde{t}}}{2\pi\sqrt{\widetilde{t}_1^2 - \frac{|\widetilde{\boldsymbol{x}}_1|^2}{c_0^2}}} \mathrm{d}\widetilde{t}_1 \mathrm{d}\widetilde{\boldsymbol{x}}_1$$

$$= \int_{\mathbb{R}^2} s(\boldsymbol{A}^{-1}(\widetilde{\boldsymbol{x}}-\widetilde{\boldsymbol{x}}_1)) e^{-i\omega(\frac{1}{\alpha}\widetilde{t} - \frac{1}{\alpha c_0}\boldsymbol{M_0}\cdot\widetilde{\boldsymbol{x}})} e^{-i\frac{\omega}{\alpha c_0}\boldsymbol{M_0}\cdot\widetilde{\boldsymbol{x}}_1} \left[\frac{i}{4} H_0^{(1)}\left(\frac{\omega}{\alpha c_0}|\widetilde{\boldsymbol{x}}_1|\right) + \mathfrak{r}_{\mathrm{conv}}\right] \mathrm{d}\widetilde{\boldsymbol{x}}_1$$

$$= \int_{\mathbb{R}^2} \frac{1}{\alpha} s(\boldsymbol{x}-\boldsymbol{x}_1) e^{-i\omega t} e^{-i\frac{\omega}{\alpha^2 c_0}\boldsymbol{M_0}\cdot\boldsymbol{x}_1} \frac{i}{4} H_0^{(1)}\left(\frac{\omega}{\alpha c_0}|\boldsymbol{A}\boldsymbol{x}_1|\right) \mathrm{d}\boldsymbol{x}_1 + \mathfrak{R}_{\mathrm{conv}},$$

where $\mathfrak{r}_{\text{conv}}$ and $\mathfrak{R}_{\text{conv}}$ are defined as $\mathfrak{r}_{\text{std}}$ and $\mathfrak{R}_{\text{std}}$ in the previous step. By using similar arguments to the ones in the previous step, we can show that

$$\lim_{t\to+\infty} \|\mathfrak{R}_{\text{conv}}(\cdot,t)\| = 0.$$

We now define the time-harmonic Green function by

$$W_{\text{conv}}(\boldsymbol{x},\omega) = \frac{1}{\alpha}\exp\left[-\frac{i\omega}{\alpha^2 c_0}\boldsymbol{M_0}\cdot\boldsymbol{x}\right]\frac{i}{4}H_0^{(1)}\left(\frac{\omega}{\alpha c_0}|\boldsymbol{A}\boldsymbol{x}|\right),$$

and we can also obtain the limiting amplitude principle for the convected Helmholtz equatio

$$\lim_{t\to\infty}\left\|p(\boldsymbol{x},t) - p_{\text{conv},\omega}(\boldsymbol{x})e^{-i\omega t}\right\| = 0,$$

where $p_{\text{conv},\omega} = W_{\text{conv}}(\cdot,\omega) * s$ is the outgoing solution of the convected Helmholtz equation.

Step 4: Equivalence under *Prandtl-Glauert-Lorentz transformation.*

We notice that

$$W_{\text{conv}}(\boldsymbol{x},\omega) = \frac{1}{\alpha}\exp\left[-\frac{i\omega}{\alpha^2 c_0}\boldsymbol{M_0}\cdot\boldsymbol{x}\right]\frac{i}{4}H_0^{(1)}\left(\frac{\omega}{\alpha c_0}|\boldsymbol{A}\boldsymbol{x}|\right) = \frac{1}{\alpha}\exp\left[-\frac{i\omega}{\alpha^2 c_0}\boldsymbol{M_0}\cdot\boldsymbol{x}\right]W_{\text{std}}\left(\widetilde{\boldsymbol{x}},\frac{\omega}{\alpha}\right),$$

We recall that $\widetilde{s}$ is defined by

$$\widetilde{s}(\widetilde{\boldsymbol{x}},\widetilde{\omega}) := \alpha\exp\left[i\omega\frac{\boldsymbol{M_0}\cdot\boldsymbol{x}}{\alpha^2 c_0}\right]s(\boldsymbol{x},\omega),$$

and we define

$$\widetilde{p}_{\text{std},\widetilde{\omega}} := W_{\text{std}}(\cdot,\widetilde{\omega}) * \widetilde{s} = \int_{\mathbb{R}^2}\widetilde{s}(\cdot-\widetilde{\boldsymbol{x}}_1)W_{\text{std}}(\widetilde{\boldsymbol{x}}_1,\widetilde{\omega})\mathrm{d}\widetilde{\boldsymbol{x}}_1.$$

We have

$$\widetilde{p}_{\text{std},\widetilde{\omega}}(\widetilde{\boldsymbol{x}}) = \alpha\exp\left[i\omega\frac{\boldsymbol{M_0}\cdot\boldsymbol{x}}{\alpha^2 c_0}\right]p_{\text{conv},\omega}(\boldsymbol{x}),$$

indeed

$$\begin{aligned}
\widetilde{p}_{\text{std},\widetilde{\omega}}(\widetilde{\boldsymbol{x}}) &= \int_{\mathbb{R}^2}\widetilde{s}(\widetilde{\boldsymbol{x}}-\widetilde{\boldsymbol{x}}_1)W_{\text{std}}(\widetilde{\boldsymbol{x}}_1,\widetilde{\omega})\mathrm{d}\widetilde{\boldsymbol{x}}_1,\\
&= \int_{\mathbb{R}^2}\alpha\exp\left[i\omega\frac{\boldsymbol{M_0}\cdot(\boldsymbol{x}-\boldsymbol{x}_1)}{\alpha^2 c_0}\right]s(\boldsymbol{x}-\boldsymbol{x}_1)\alpha\exp\left[i\omega\frac{\boldsymbol{M_0}\cdot\boldsymbol{x}_1}{\alpha^2 c_0}\right]W_{\text{conv}}(\boldsymbol{x}_1,\omega)\frac{\mathrm{d}\boldsymbol{x}_1}{\alpha},\\
&= \alpha\exp\left[i\omega\frac{\boldsymbol{M_0}\cdot\boldsymbol{x}}{\alpha^2 c_0}\right]\int_{\mathbb{R}^2}s(\boldsymbol{x}-\boldsymbol{x}_1)W_{\text{conv}}(\boldsymbol{x}_1,\omega)\mathrm{d}\boldsymbol{x}_1.
\end{aligned}$$

So the outgoing solutions are mapped to one another through the *Prandtl-Glauert-Lorentz transformation.*

■

Appendix B. Plane-wave solutions of the convected Helmholtz equation

We compute the plane waves for the system (1). We write p as

$$p = p_0 e^{i\boldsymbol{\kappa}\cdot\boldsymbol{x}}$$

with $p_0 \in \mathbb{C}$.

We can rewrite (1) as

$$p_0 \left[-\omega + 2\omega \boldsymbol{v_0}\cdot\boldsymbol{\kappa} + \boldsymbol{\kappa}^T \boldsymbol{K_0}\boldsymbol{\kappa}\right] = 0,$$

and therefore

$$-\rho_0\omega^2 + 2\omega\rho_0 \boldsymbol{v_0}\cdot\boldsymbol{\kappa} + \rho_0 c_0^2 |\boldsymbol{\kappa}|^2 - \rho_0(\boldsymbol{v_0}\cdot\boldsymbol{\kappa})^2 = 0. \tag{B.1}$$

As we only have one equation for two unknowns, we make the following assumptions

$$\begin{aligned} \boldsymbol{\kappa} &:= \kappa \begin{bmatrix}\cos\theta \\ \sin\theta\end{bmatrix}, && \text{where } \theta \in [0, 2\pi) \text{ is assumed to be known,} \\ \boldsymbol{v_0} &:= Mc_0 \begin{bmatrix}\cos\theta_0 \\ \sin\theta_0\end{bmatrix}, && \text{where } \theta_0 \in [0, 2\pi). \end{aligned}$$

With those assumptions, (B.1) becomes

$$-\omega^2 + 2\omega\kappa M c_0 \left(\cos\theta_0\cos\theta + \sin\theta_0\sin\theta\right) + c_0^2\kappa^2 - M^2 c_0^2 \kappa^2 \left(\cos\theta_0\cos\theta + \sin\theta_0\sin\theta\right)^2 = 0,$$

or equivalently

$$-\omega^2 + 2\omega\kappa M c_0 \cos(\theta - \theta_0) + c_0^2\kappa^2 \left(1 - M^2\cos^2(\theta - \theta_0)\right) = 0.$$

Solving this last equation for κ leads to the two following solutions

$$\kappa_- = \frac{-\omega}{c_0(1 - M\cos(\theta - \theta_0))} \quad \text{and} \quad \kappa_+ = \frac{\omega}{c_0(1 + M\cos(\theta - \theta_0))}.$$

Notice that $\boldsymbol{\kappa}$ can be rewritten as

$$\boldsymbol{\kappa} = \frac{\kappa_\pm}{Mc_0}\left(\cos(\theta - \theta_0)\boldsymbol{v_0} + \sin(\theta - \theta_0)\boldsymbol{v_0^\perp}\right).$$

We can therefore rewrite $\boldsymbol{\sigma}$ as

$$\boldsymbol{\sigma}\cdot\boldsymbol{n} = -i\omega c_0 \left(1 \pm M\cos(\theta - \theta_0)\right) p = -i\omega\left(c_0 \pm \boldsymbol{v_0}\cdot\boldsymbol{n}\right) p.$$

[ABB99] X. Antoine, H. Barucq, and A. Bendali. Bayliss-Turkel-like Radiation Condition on Surfaces of Arbitrary Shape. *Journal of Mathematical Analysis and Applications*, 229(1):184–211, 1999. Cited on pages 10 and 26.

[BBJ02] C. Bogey, C. Bailly, and D. Juvé. Computation of Flow Noise Using Source Terms in Linearized Euler's Equations. *Aiaa Journal - AIAA J*, 40:235–243, February 2002. Cited on page 26.

[BBL03] E. Bécache, A.S. Bonnet-Ben Dhia, and G. Legendre. Perfectly matched layers for the convected Helmholtz equation. Technical report, 2003. Cited on pages 2 and 25.

[BCD+14] N. Balin, F. Casenave, F. Dubois, E. Duceau, S. Duprey, and I. Terrasse. Boundary Element and Finite Element Coupling for Aeroacoustics Simulations. Technical report, February 2014. Cited on pages 2 and 24.

[Ber94] J.P. Berenger. A perfectly matched layer for the absorption of electromagnetic waves. *Journal of Computational Physics*, 114(2):185–200, October 1994. Cited on page 1.

[Bér08] H. Bériot. *Eléments Finis d'ordre Élévé Pour l'opérateur de Galbrun En Régime Harmonique*. Thesis, Compiègne, January 2008. Cited on page 25.

[BMM+12] A.S. Bonnet-Ben Dhia, J.F. Mercier, F. Millot, S. Pernet, and E. Peynaud. Time-Harmonic Acoustic Scattering in a Complex Flow: A Full Coupling Between Acoustics and Hydrodynamics. *Communications in Computational Physics*, 11(2):555–572, February 2012. Cited on page 26.

[BRT21] H. Barucq, N. Rouxelin, and S. Tordeux. HDG and HDG+ methods for harmonic wave problems with convection. 2021. Cited on pages 5, 13, and 16.

[BST12] H. Barucq, A.-G. Dupouy St-Guirons, and S. Tordeux. Non-reflecting boundary condition on ellipsoidal boundary. *Numerical Analysis and Applications*, 5(2):109–115, April 2012. Cited on page 10.

[BT80] A. Bayliss and E. Turkel. Radiation boundary conditions for wave-like equations. *Communications on Pure and Applied Mathematics*, 33(6):707–725, 1980. Cited on page 10.

[CES14] F. Casenave, A. Ern, and G. Sylvand. Coupled BEM–FEM for the convected Helmholtz equation with non-uniform flow in a bounded domain. *Journal of Computational Physics*, 257:627–644, January 2014. Cited on page 2.

[DJ06] J. Diaz and P. Joly. A time domain analysis of PML models in acoustics. *Computer Methods in Applied Mechanics and Engineering*, 195(29-32):3820–3853, June 2006. Cited on pages 2, 26, and 27.

[EM77] B. Engquist and A. Majda. Absorbing Boundary Conditions for the Numerical Simulation of Waves. *Mathematics of Computation*, page 23, 1977. Cited on pages 1, 2, and 14.

[Fau21] F. Faucher. 'hawen': Time-harmonic wave modeling and inversion using hybridizable discontinuous Galerkin discretization. *Journal of Open Source Software*, 6(57):2699, January 2021. Cited on page 16.

[Gab03] G. Gabard. *Méthodes Numériques et Modèles de Sources Aéroacoustiques Fondées Sur l'équation de Galbrun*. PhD thesis, 2003. Cited on page 25.

[HPN17] F. Hu, M. Pizzo, and D. Nark. On a time domain boundary integral equation formulation for acoustic scattering by rigid bodies in uniform mean flow. *The Journal of the Acoustical Society of America*, 142(6):3624, December 2017. Cited on page 3.

[HPN19] F. Hu, M. Pizzo, and D. Nark. On the use of a Prandtl-Glauert-Lorentz transformation for acoustic scattering by rigid bodies with a uniform flow. *Journal of Sound and Vibration*, 443:198–211, March 2019. Cited on pages 2, 3, 7, 11, and 12.

[Kim14] S. Kim. Analysis of the convected Helmholtz equation with a uniform mean flow in a waveguide with complete radiation boundary conditions. *Journal of Mathematical Analysis and Applications*, 410(1):275–291, February 2014. Cited on page 2.

[KSC12] R. Kirby, S. Sherwin, and B. Cockburn. To CG or to HDG: A Comparative Study. *Journal of Scientific Computing*, 51(1):183–212, April 2012. Cited on page 16.

[LMG+20] A. Lieu, P. Marchner, G. Gabard, H. Beriot, X. Antoine, and C. Geuzaine. A Non-Overlapping Schwarz Domain Decomposition Method with High-Order Finite Elements for Flow Acoustics. *Computer Methods in Applied Mechanics and Engineering*, 2020. Cited on pages 3 and 24.

[MAGB21] P. Marchner, X. Antoine, C. Geuzaine, and H. Bériot. Construction and Numerical Assessment of Local Absorbing Boundary Conditions for Heterogeneous Time-Harmonic Acoustic Problems. April 2021. Cited on pages 2 and 26.

[MBAG20] P. Marchner, H. Beriot, X. Antoine, and C. Geuzaine. Stable Perfectly Matched Layers with Lorentz transformation for the convected Helmholtz equation. Technical report, 2020. Cited on pages 2 and 25.

[MMMP17] J.F. Mercier, C. Mietka, F. Millot, and V. Pagneux. Acoustic propagation in a vortical homentropic flow. page 19, 2017. Cited on page 26.

[OLBC10] F. Olver, D. Lozier, R. Boisvert, and C. Clark. NIST Handbook of Mathematical Functions. January 2010. Cited on page 28.

[Pie90] A. Pierce. Wave equation for sound in fluids with unsteady inhomogeneous flow. *The Journal of the Acoustical Society of America*, 87(6):2292–2299, June 1990. Cited on page 3.

[Pro59] M. H. Protter. Unique continuation for elliptic equations. 1959. Cited on page 6.

[Sai08] A.G. Saint-Guirons. *Construction et Analyse de Conditions Absorbantes de Type Diritchlet-to-Neumann Pour Des Frontières Ellipsoïdales*. PhD Thesis, Pau, January 2008. Cited on page 10.

[SM50] J. Sherman and W. Morrison. Adjustment of an Inverse Matrix Corresponding to a Change in One Element of a Given Matrix. *Annals of Mathematical Statistics*, 21(1):124–127, March 1950. Cited on page 7.

[Ver10] A. Verruijt. *An Introduction to Soil Dynamics*. Theory and Applications of Transport in Porous Media. Springer Netherlands, 2010. Cited on page 27.